bioRxiv preprint doi: https://doi.org/10.1101/2021.05.09.443283; this version posted May 9, 2021. The copyright holder for this preprint (which was not certified by peer review) is the author/funder, who has granted bioRxiv a license to display the preprint in perpetuity. It is made available under aCC-BY-NC-ND 4.0 International license.

Glutathione regulates subcellular iron homeostasis via transcriptional activation of iron responsive genes in Arabidopsis

Ranjana Shee[1,2], Soumi Ghosh[1,$], Pinki Khan[1,$], Salman Sahid[1,2], Chandan Roy[2], Dibyendu Shee[2], Soumitra Paul[2*], Riddhi Datta[1*]

[1]Department of Botany, Dr A. P. J. Abdul Kalam Government College, New Town, Kolkata 700156

[2]Department of Botany, University of Calcutta, 35, Ballygunge Circular Road, Kolkata 700019, West Bengal, India

Email addresses:

Ranjana Shee: ranjana.shee22@gmail.com, Soumi Ghosh: soumimpplab@gmail.com, Pinki Khan: pinkimpplab@gmail.com, Salman Sahid: salmansahid1991@gmail.com, Chandan Roy: suchandan.roy35@gmail.com, Dibyendu Shee: dibyendushee01@gmail.com, Soumitra Paul: psoumitra@ymail.com, Riddhi Datta: riddhi.bot@gmail.com

*****Authors for correspondence:

Email: psoumitra@ymail.com, riddhi.bot@gmail.com; Telephone No: +919748605305, +919433084074

[$]These authors contributed equally

Date of submission: 09.05.2021

Number of figures: 10; colour in on-line: 3

Word count: 4378

Total Supplementary Data: 9, Supplementary Figures: 7, Supplementary Tables: 2

Running title**: GSH regulates subcellular iron homeostasis in Arabidopsis**

Highlight

Glutathione regulates subcellular iron homeostasis under iron deficiency via GSNO dependent transcriptional activation of *AtNRAMP3*, *AtNRAMP4*, *AtPIC1*, *AtFer1* and *AtIRT1* genes presumably by *S*-nitrosylation of different iron responsive bHLH factors.

bioRxiv preprint doi: https://doi.org/10.1101/2021.05.09.443283; this version posted May 9, 2021. The copyright holder for this preprint (which was not certified by peer review) is the author/funder, who has granted bioRxiv a license to display the preprint in perpetuity. It is made available under aCC-BY-NC-ND 4.0 International license.

Abstract

Glutathione (GSH) is a ubiquitous molecule known to regulate various physiological and developmental phenomena in plants. Recently, its involvement in regulating iron (Fe) deficiency response was established in Arabidopsis. However, the role of GSH in modulating subcellular Fe homeostasis remained elusive. In this study, we dissected the role of GSH in regulating Fe homeostasis in Arabidopsis shoots under Fe limited conditions. The two GSH depleted mutants, *cad2-1* and *pad2-1* displayed increased sensitivity to Fe deficiency with smaller rosette diameter and higher chlorosis level compared with the Col-0 plants. Interestingly, the expression of the vacuolar Fe exporters, *AtNRAMP*3 and *AtNRAMP*4, chloroplast Fe importer, *AtPIC*1, along with *AtFer*1 and *AtIRT*1 were significantly down-regulated in these mutants. The expression of these genes were up-regulated in response to exogenous GSH treatment while treatment with BSO, a GSH inhibitor, down-regulated their expression. Moreover, the mutants accumulated higher Fe content in the vacuole and lower in the chloroplast compared with Col-0 under Fe limited condition suggesting a role of GSH in modulating subcellular Fe homeostasis. This regulation was, further, found to involve a GSNO-dependent pathway. Promoter analysis revealed that GSH induced the transcription of these genes presumably via *S*-nitrosylation of different Fe responsive bHLH transcription factors.

Keywords: Glutathione, iron deficiency, subcellular iron homeostasis, GSNO, NRAMP, PIC, ferritin

bioRxiv preprint doi: https://doi.org/10.1101/2021.05.09.443283; this version posted May 9, 2021. The copyright holder for this preprint (which was not certified by peer review) is the author/funder, who has granted bioRxiv a license to display the preprint in perpetuity. It is made available under aCC-BY-NC-ND 4.0 International license.

Introduction

Iron (Fe) is an essential micronutrient for plant growth and development. It plays an important role in regulating numerous cellular responses because of its physicochemical properties. This micronutrient is known to coordinate metalloprotein active sites and regulate many important enzymatic reactions required for nitrogen fixation, DNA synthesis and biosynthesis of various phytohormones (Briat *et al*., 2015). Although Fe is found abundantly in the earth's crust, it is usually present in an oxidized form and its availability to plants is limited. The deficiency of Fe in plants causes chlorosis and perturbs photosynthesis and oxidative phosphorylation by hampering different electron carriers of photosynthetic machineries as well as mitochondrial electron transport system. Therefore, Fe deficiency is a challenging issue for plant growth, development and productivity.

Plants have evolved highly sophisticated mechanisms for Fe uptake and transport. Two basic strategies for Fe uptake are described in the graminecious and non-graminecious plants (Morrissey and Guerinot, 2009). Among them, the strategy I or reduction based strategy is found in the non-graminecious plants like *Arabidopsis* where the plasmamembrane H^+-ATPases (AHAs) release protons to increase rhizosphere acidification. This promotes the reduction of Fe^{3+} to the more soluble Fe^{2+} by ferric reductase oxidase 2 (FRO2) (Robinson *et al*., 1999). Iron regulated transporter 1 (IRT1), a member of the ZIP metal transporter family, imports the reduced Fe^{2+} into the root cells (Vert *et al*., 2002). Also, shoot specific FRO7 plays an important role in Fe delivery to chloroplasts. Besides, FRO3 and FRO8, present in the mitochondrial membrane, also regulate Fe homeostasis in mitochondria (Jeong and Connolly, 2009).

Modulating intracellular Fe homeostasis is crucial particularly under altered Fe conditions and involves several Fe transporters. A high-affinity Fe transporter, natural resistance against macrophage protein (NRAMP), having significant similarity with its mammalian counterpart, was identified in *A. thaliana* (Curie *et al*., 2000). Although their functional role in plants was not entirely revealed, complementation assays in yeast showed that these proteins were induced under Fe deficient condition. NRAMP 1, 3 and 4 represent multi-specific metal transporters localized in roots and leaves (Curie *et al*. 2000; Thomine *et al*. 2003; Lanquar *et al*., 2005). In Arabidopsis, NRAMP3 and NRAMP4 were identified to retrieve and export Fe from vacuoles to chloroplast during the Fe deficient condition (Bastow *et al*., 2018). In fact, the vacuolar Fe released by these two transporters was found to be the primary source of Fe

bioRxiv preprint doi: https://doi.org/10.1101/2021.05.09.443283; this version posted May 9, 2021. The copyright holder for this preprint (which was not certified by peer review) is the author/funder, who has granted bioRxiv a license to display the preprint in perpetuity. It is made available under aCC-BY-NC-ND 4.0 International license.

in germinating seeds (Bastow *et al*., 2018). On the other hand, vacuolar iron transporter 1 (VIT1) was identified as one of the key transporters involved in Fe influx into the vacuole. It thus functions in the vacuolar sequestration process essential for detoxification under the excess Fe condition (Kim *et al*., 2006). In plants, maintaining the plastidal Fe homeostasis is crucial for survival. Several Fe transporters like permease in chloroplasts 1 (PIC1), non-intrinsic ABC protein 11 (NAP11) and NAP14 were identified as Fe importers that transport Fe across the chloroplast envelope (Duy *et al*., 2007; Shimoni-Shor *et al*., 2010). On the other hand, several transporters like yellow stripe like 1 (YSL1) and YSL3 help in maintaining Fe homeostasis by regulating Fe efflux from the chloroplast (Waters *et al*., 2006; Chu *et al*., 2010).

Glutathione (GSH) is a multifunctional metabolite that has drawn extensive attention due to its unique structural properties, abundance, broad redox potential, and wide distribution in most living organisms. Along with ascorbate, GSH is considered as one of the most abundant redox couples in plant cells (Foyer and Halliwell, 1976). In plants, GSH is known to play a pivotal role in regulating stress responses as well as growth and development. Phenotypic analysis of GSH deficient Arabidopsis mutants demonstrated that GSH was essentially required for plant development, particularly embryo and meristem development (Vernoux *et al*., 2000; Cairns *et al*., 2006; Reichheld *et al*., 2007; Frottin *et al*., 2009; Bashandy *et al*., 2010). The *rml1* mutant, which was severely deficient in GSH, developed non-functional root meristem while the shoot meristem remained largely unaffected (Vernoux *et al*., 2000). In addition to serving as a source of reduced sulfur during secondary metabolite biosynthesis, GSH was widely reported to play crucial role in plant defense signalling network. Ball *et al*. (2004) reported that several stress responsive genes were altered due to changed GSH metabolism in *A. thaliana rax1-1* and *cad2-1* mutants of GSH biosynthesis enzyme. Another GSH deficient mutant, *pad2-1*, was demonstrated to be susceptible to *Pseudomonas syringae* as well as *P. brassicae* infections (Glazebrook and Ausubel, 1994; Glazebrook *et al*., 1997; Parisy *et al*., 2007; Datta and Chattopadhyay, 2015). Besides, GSH was shown to be involved in the modulation of NPR1-dependent and independent salicylic acid signalling pathways (Ghanta *et al*., 2011; Han *et al*., 2013). Subsequently it was reported that GSH induces ethylene biosynthetic pathway via transcriptional as well as post transcriptional regulation of the key enzymes (Datta *et al*., 2015).

bioRxiv preprint doi: https://doi.org/10.1101/2021.05.09.443283; this version posted May 9, 2021. The copyright holder for this preprint (which was not certified by peer review) is the author/funder, who has granted bioRxiv a license to display the preprint in perpetuity. It is made available under aCC-BY-NC-ND 4.0 International license.

Again, GSH exhibits a wide range of metal chelating activities and plays important role to reduce metal toxicity in plants. Detoxification of heavy metals within plant cell occurs via phytochelatins (PCs) that are synthesized from GSH by the enzyme phytochelatin synthase (Grill *et al*., 1989; Clemens *et al*., 1999; Vatamaniuk *et al*., 1999). On cadmium or copper exposure *A. thaliana* plants responded by increasing the transcription of *glutathione synthetase* and *glutathione reductase* (*GR*) genes which were involved in GSH synthesis and reduction respectively (Queval *et al*., 2009). Further, the involvement of GSH was reported in combating metal toxicity against arsenic stress in maize (Requejo and Tena, 2012), chromium toxicity in rice (Zeng *et al*., 2012; Qiu *et al*., 2013) and cadmium stress in *Pinus* and *A. thaliana* (Schützendübel *et al*., 2001; Jobe *et al*., 2012). Cross-talk of GSH with zinc and Fe homeostasis was also reported (Shanmugam *et al*., 2012). In another study, GSH was reported to trigger the upregulation of genes related to Fe uptake and transport and to increase the Fe concentration in *A. thaliana* seedlings under Fe deficiency (Koen *et al*., 2012). GSH-ascorbate redox cycle was studied against Fe deficiency as well (Ramírez *et al*., 2013). Previous studies demonstrated the association of GSH in maturation of Fe-S molecule and transport of dinitrosyl-Fe complexes in plants (Hider and Kong, 2011; Kumar *et al*., 2011). GSH also served as the reservoir of nitric acid (NO) by formation of S-nitrosoglutathione (GSNO) complex which helped in NO mediated signalling including Fe deficiency responses (Chen *et al*., 2010; Ramirez *et al*., 2011). Subsequently, Shanmugam *et al*. (2015) revealed the role of GSH in enhancement of Fe deficiency tolerance in plants. The activities of several Fe related transporters like *AtIRT1*, *AtFRO2* and *AtFIT* was reduced in *zir1*, a GSH depleted mutant of Arabidopsis, compared to the wild-type (WT). This observation attributed the role of GSH in regulation of Fe transport under Fe-limiting condition. However, the involvement of GSH in modulating subcellular Fe homeostasis in shoot has not been elucidated so far.

In this study, we report that the two GSH depleted mutants, *cad2-1* and *pad2-1* displayed increased sensitivity towards Fe deficiency. Several organellar Fe transporters, viz. *At*NRAMP3, *At*NRAMP4, *At*PIC1 as well as *At*Fer1 were found to be down-regulated in both the mutants in addition to *At*IRT1. This GSH mediated regulation involved transcriptional activation of the identified genes presumably via *S*-nitrosylation of different Fe responsive bHLH transcription factors.

Materials and methods:

Plant growth, stress treatment and morphological analysis

bioRxiv preprint doi: https://doi.org/10.1101/2021.05.09.443283; this version posted May 9, 2021. The copyright holder for this preprint (which was not certified by peer review) is the author/funder, who has granted bioRxiv a license to display the preprint in perpetuity. It is made available under aCC-BY-NC-ND 4.0 International license.

The seeds of *A. thaliana* Columbia ecotype (Col-0) along with 2 GSH depleted mutants, *cad2-1* and *pad2-1*, were procured from Nottingham Arabidopsis Stock Centre, UK. The seeds were inoculated in MS medium (Murashige and Skoog, 1962) after surface sterilization with 4 % sodium hypochlorite and Tween 20. The plants were maintained at 21°C with 60 % relative humidity and a photoperiod of 16 h light/8 h dark cycles (Datta *et al*., 2015).

The 7 d old seedlings were transferred to either minimal iron (MI) or depleted iron (DI) medium and maintained for 7 d. The MI medium contained 10 μM Fe in contrast to 100 μM Fe in the MS medium. For preparation of DI medium, the Fe salt was omitted from MS medium keeping all other components unaltered. In addition, 300 μM ferrozine [3-(2-pyridyl)-5,6-diphenyl-1,2,4- triazine sulfonate] was also added to remove any trace amount of Fe from the medium (Eroglu *et al.*, 2016). For control set, seedlings were maintained in MS medium for the entire period. After 7 d of stress treatment, the morphological parameters including primary root length, lateral root density and rosette diameter were measured using Image J software.

RNA extraction and quantitative-RT PCR analysis

Total RNA was isolated from the tissue samples by Trizol method. Complementary DNA (cDNA) was prepared subsequently using iScript™ cDNA Synthesis Kit (Bio-rad) following manufacturer's protocol. Quantitative PCR amplification was carried out in CFX96 Touch™ Real-Time PCR Detection System (Bio-rad) using iTaq™ Universal SYBR® Green Supermix (Bio-rad) and gene specific primers (Supplementary Table S1). *AtActin2* was used as a reference gene to normalize the relative expression and *AtIRT*1 was used as Fe-responsive marker gene to confirm the Fe deficient conditions.

Chemical treatment of seedlings

15 d old seedlings were used for chemical treatments. For GSH feeding, freshly prepared 100 μM GSH was used while for BSO treatment, 1 mM BSO was used for 72 h as standardized before (Datta *et al.*, 2015). For DTT treatment, a 5 mM DTT solution was used for 24 h treatment. In case of GSNO feeding, the seedlings were treated with 250 μM GSNO for 72 h (Kailasham et al., 2018). For tungstate treatment, seedlings were treated with 1 mM sodium tungstate for 72 h (Chen et al., 2010). Control seedlings were maintained in half strength MS medium.

Estimation of Fe content

bioRxiv preprint doi: https://doi.org/10.1101/2021.05.09.443283; this version posted May 9, 2021. The copyright holder for this preprint (which was not certified by peer review) is the author/funder, who has granted bioRxiv a license to display the preprint in perpetuity. It is made available under aCC-BY-NC-ND 4.0 International license.

Fe content from different tissues was measured through dry ash digestion method with slight modifications (Jiang *et al*., 2007). Briefly, tissues were harvested from 15 d old seedlings, washed with HPLC grade water, pat dried, weighed and used for ash preparation. The ash was digested with 0.5 M HNO_3 and filtered through Whatman no. 42 filters. The solution was again filtered through Millex® GV 0.22 µm PVDF membrane filter (Merck Millipore). The Fe content was analysed using ICP-OES (iCAP 6300 Duo ICP-OES, Thermo Scientific).

Estimation of Chlorophyll content

The chlorophyll content was estimated following Lichtenthaler (1987). Briefly, 200 mg tissue was homogenized in 80 % acetone, followed by centrifugation at 5000 g for 5 min. The supernatant was used for the estimation of total chlorophyll.

Estimation of total GSH content and GSH:GSSG ratio

GSH estimation was performed following Anderson (1985). Briefly, 200 mg of tissue was homogenized in 5 % sulphosalicylic acid followed by centrifugation at 12000 g for 20 min. GSH was estimated from the supernatant by 5,5'-dithiobis-(2-nitrobenzoic acid) (DTNB) method. For estimation of total GSH, 0.4 mM NADPH and GR were added to the reaction buffer. Optical density was measured at 412 nm using a Double Beam UV-Vis Spectrophotometer (U2900, Hitachi). Amount of GSSG was calculated by subtracting GSH amount from total GSH.

Isolation of chloroplast and vacuole

Chloroplast was isolated from leaves as standardized before (Kleffmann *et al*., 2004; Ghanta *et al*., 2014). Briefly, leaves were finely chopped in chloroplast extraction buffer (0.3 M sorbitol, 1 mM $MgCl_2$, 50 mM HEPES/KOH, 2 mM EDTA, 0.04 % β-marcaptoethanol, 0.1 % PVPP, pH 7.8), filtered and centrifuged at 4 °C for 10 min at 1300 g. The pellet was suspended in isolation buffer (0.3 M sorbitol, 1 mM $MgCl_2$, 50 mM HEPES/KOH, 2 mM EDTA, pH 7.8). The solution was loaded on the top of percoll gradient and centrifuged at 4 °C and 8000 g for 20 min. Intact chloroplasts were isolated and washed twice with the isolation buffer.

Vacuoles were isolated from leaves following Zouhar (2016). Briefly, leaves were collected, weighed, cut with razor blade into 2 mm strips and immersed in the protoplast isolation buffer [(1 % (w/v) Cellulase R10, 1 % (w/v) Macerozyme R10, 0.4 M mannitol, 25 mM

bioRxiv preprint doi: https://doi.org/10.1101/2021.05.09.443283; this version posted May 9, 2021. The copyright holder for this preprint (which was not certified by peer review) is the author/funder, who has granted bioRxiv a license to display the preprint in perpetuity. It is made available under aCC-BY-NC-ND 4.0 International license.

$CaCl_2$, 5 mM β-mercaptoethanol, 10 mM 2-[N-morpholino]ethanesulfonic acid (MES)-KOH, (pH 5.7)]. The solution was then infiltrated and incubated for 4 h at room temperature with continuous shaking. The released protoplasts were filtered followed by centrifugation at 80 g at 20 °C for 15 min. 10 % Ficoll buffer was added to the pellet for protoplast disruption. The lysed protoplast solution was then treated with 4 % Ficoll buffer followed by vacuole isolation buffer (0.45 M mannitol, 5 mM sodium phosphate, 2 mM EDTA, pH 7.5). The solution was then ultracentrifuged at 50,000 g for 50 min at 10 °C. Vacuoles were collected from the 4 % Ficoll buffer/vacuole buffer interface.

The isolated chloroplast and vacuole fractions were used for Fe estimation as described above.

Fe localization by Perls prussian blue and DAB staining

The Fe localization using Perls prussian blue staining technique was carried out following Rochhartdz *et al*. (2009). Briefly, the plant samples were fixed in a 6:3:1 methanol:chloroform:acetic acid (v/v) solution and washed twice with ultrapure water. The plants were then transferred to the pre-warmed staining solution (4 % (w/v) $K_4Fe(CN)_6$ and 4 % (v/v) HCl) and incubated at room temperature for 1 h. After removing the staining solution, the samples were washed twice with ultrapure water. For DAB intensification, the samples were incubated in preparation solution (0.01 M Na_2CO_3 and 0.3 % H_2O_2 in methanol) for 1 h. After washing with the 0.1 M phosphate buffer (pH 7) the samples were incubated in intensification solution (0.025 % (v/v) H_2O_2 and 0.005 % (w/v) $CaCl_2$) and kept at room temperature for 30 min. The samples were then washed with ultrapure water and photographed.

Vector construction and raising of transformed Arabidopsis plants

Genomic DNA was extracted from shoots following CTAB method. To clone the promoter regions of *AtIRT1*, *AtFer1*, *AtPIC1*, *AtNRAMP3* and *AtNRAMP4* genes, approximately 1.5 kb of intergenic region upstream of the transcription start site was amplified by PCR using gene specific primers (Supplementary Table S1). The amplified promoter regions were cloned into pCAMBIA1304 between *BamHI* and *BglII* restriction enzyme sites to generate *AtIRT1pro*::*GUS*, *AtNRAMP3pro*::*GUS and AtNRAMP4pro*::*GUS* constructs and between *BamHI* and *SpeI* to produce *AtPIC1pro*::*GUS* and *AtFer1pro*::*GUS* constructs. These constructs were then transformed into Col-0 plants through *Agrobacterium* mediated floral

bioRxiv preprint doi: https://doi.org/10.1101/2021.05.09.443283; this version posted May 9, 2021. The copyright holder for this preprint (which was not certified by peer review) is the author/funder, who has granted bioRxiv a license to display the preprint in perpetuity. It is made available under aCC-BY-NC-ND 4.0 International license.

dip transformation method (Clough and Bent, 1998). A vector control line harbouring the *CaMV35S::GUS* construct was generated as well. The transformed lines harbouring the recombinant constructs were selected and maintained up to T_2 generations in a growth chamber as described above.

Histochemical GUS assay

The seedlings from the transgenic lines harbouring the *AtIRT1pro*::*GUS*, *AtFer1pro*::*GUS*, *AtPIC1pro*::*GUS*, *AtNRAMP3pro*::*GUS*, *AtNRAMP4pro*::*GUS* and *CaMV35S::GUS* constructs were incubated under DI condition or fed with GSH and GSNO as described above. The samples were then infiltrated with GUS staining solution (0.5 mg mL^{-1} 5-bromo-4-chloro-3-indolyl-β-D-glucuronic acid, 0.5 mM potassium ferrocyanide, 0.5 mM potassium ferricyanide, 0.1 % (v/v) Triton X-100, 100 mM phosphate buffer, pH 7.0, and 10 mM EDTA) following Jefferson *et al*. (1987). The stained samples were washed with 70 % ethanol and photographed.

In silico prediction of S-nitrosylation sites

The 12 basic helix loop helix (bHLH)) transcription factors (TFs) like *At*bHLH6, *At*bHLH11, *At*bHLH18, *At*bHLH19, *At*bHLH20, *At*bHLH25, *At*bHLH34, *At*bHLH47 (POPEYE), *At*bHLH104, *At*bHLH105, *At*bHLH115, and *At*bHLH121 were considered in this study and their protein sequences were retrieved from UniProt database (http://www.uniprot.org/uniprot/). These sequences were submitted to GPS-SNO 1.0 software to predict the presence of *S*-nitrosylated cysteine residues using threshold level as high (Xue *et al*., 2010). The cysteine (cys/c) residues which undergo *S*-nitrosylation were considered as positive hits (+) while the non-nitrosylated cysteine residues were considered as negative hits (-). The enrichment for *S*-nitrosylated cysteine residues was depicted using CentriMo 5.3.3 web server (https://meme-suite.org/meme/tools/centrimo; Bailey and Machanick, 2012). In addition, the presence of bHLH TF binding motifs were identified in the promoter regions of *AtNRAMP3*, *AtNRAMP4*, *AtPIC1*, *AtIRT1* and *AtFER1* using PlantPan 3.0 (plantpan.itps.ncku.edu.tw/promoter.php) and MEME suite 5.3.3 (https://meme-suite.org/; Bailey *et al*., 2009).

Statistical analysis

Statistical analysis of the data was performed using GraphPad Prism version 8.3.0 software (GraphPad Software, San Diego, California USA). The variation of morphological, and

bioRxiv preprint doi: https://doi.org/10.1101/2021.05.09.443283; this version posted May 9, 2021. The copyright holder for this preprint (which was not certified by peer review) is the author/funder, who has granted bioRxiv a license to display the preprint in perpetuity. It is made available under aCC-BY-NC-ND 4.0 International license.

biochemical parameters as well as the relative transcript abundance among different samples were analyzed following two-way ANOVA followed by Sidak's multiple comparison tests. The statistical significance at $P \leq 0.05$ was considered to determine the difference between two sets of data. Details of replicates, sample size, and the significance levels of P-values were indicated in respective figure legends. The data were represented as mean ± standard error of mean (SEM).

Results

GSH depleted mutants displayed increased sensitivity to Fe deficient conditions

To explore if GSH plays a role in regulating Fe homeostasis, two GSH depleted mutants, *cad2-1* and *pad2-1*, containing only 40 % and 22 % GSH respectively, were selected for this study. The MS medium containing 100 μM Fe was used as a control medium while the MI medium containing 10 μM Fe and the DI medium lacking any Fe source and containing the Fe-chelator, ferrozine were used as Fe deficient media. Since, the expression of *AtIRT1* gene was found to be the highest after 7 d treatment, this time point was used for all downstream analyses (Supplementary Fig. S1). The mutant lines when grown under MI and DI conditions displayed increased sensitivity to Fe deficiency as compared with the Col-0 plants (Fig. 1). The rosette diameter was found to be significantly reduced in the mutants compared with the Col-0 plants after 7 d of treatment. In addition, the root morphology was also altered in response to Fe deficiency. The primary root length decreased in all 3 lines with the shortest root length in the *pad2-1* plants under both MI and DI conditions. Lateral root density was found to be considerably increased in all the 3 lines. Since Fe deficiency is widely known to affect the photosynthetic machinery, we estimated the total chlorophyll content. While all the 3 lines displayed chlorosis in response to Fe deficiency, the mutant lines showed significantly lower total chlorophyll content under both MI and DI conditions as compared with the Col-0 plants.

To determine any correlation between GSH and Fe contents, we also analyzed the total GSH content, GSH:GSSG ratio as well as the Fe content under control and Fe deficiency conditions. Interestingly, the mutant lines exhibited significantly lower Fe content in the shoot as well as the root as compared with Col-0 plants (Fig. 2A, D). The lower Fe content in the mutant lines was also visualized by Perls-DAB staining (Supplementary Fig. S2). On the other hand, the total GSH content increased under MI and DI conditions while the

bioRxiv preprint doi: https://doi.org/10.1101/2021.05.09.443283; this version posted May 9, 2021. The copyright holder for this preprint (which was not certified by peer review) is the author/funder, who has granted bioRxiv a license to display the preprint in perpetuity. It is made available under aCC-BY-NC-ND 4.0 International license.

GSH:GSSG ratio decreased. As expected, the mutant lines displayed lower GSH levels in both the shoot and the roots as compared with the Col-0 plants (Fig. 2B, C, E, F).

GSH played a crucial role in regulating Fe transporters and ferritin genes

Since the GSH depleted mutants were sensitive to Fe deficiency, the next pertinent point was to identify the Fe transporters that might be regulated by GSH. To this end, the expression of the Fe transporter genes were analyzed in the mutant lines and compared with the Col-0 plants. Interestingly, it was found that the expression of *AtNRAMP3*, *AtNRAMP4*, *AtPIC1* and *AtIRT1* genes were significantly down-regulated in the mutant lines as compared with the Col-0 plants (Fig. 3). On the other hand, the expression of *AtYSL1* and *AtYSL3* genes were found to be up-regulated in the mutant lines. Besides, several genes involved in regulating Fe homeostasis were also analyzed. Among them, *AtFer1* gene was found to be significantly down-regulated in the mutant lines as compared with the Col-0 (Fig. 4). This observation strongly suggested the involvement of GSH in modulating Fe homeostasis in plants. Since the *AtNRAMP3*, *AtNRAMP4*, *AtPIC1*, *AtFer1* and *AtIRT1* genes are known to be induced by Fe deficiency, we checked their expression under DI condition. It was found that under DI condition as well, the relative transcript abundance for all these genes were significantly lower in the mutant lines further supporting the previous observations (Fig. 5).

Exogenously altered GSH level was sufficient to regulate Fe responsive gene expression

To further confirm the GSH-mediated regulation of the identified Fe responsive genes, Col-0 seedlings were exogenously treated with GSH or an inhibitor of GSH biosynthesis, BSO. In addition, a non-specific reducing agent DTT was also used for treatment. A half strength MS medium was used as a control set. To confirm the efficiency of the feeding treatments, total GSH content was estimated from each set. The total GSH level was found to be significantly increased in the GSH-fed plants, decreased in the BSO-fed plants while no significant alteration was observed in the DTT-fed plants (Fig. 6A). Next, the relative transcript abundance of the identified genes was analyzed. It was observed that the expression of the *AtNRAMP3*, *AtNRAMP4*, *AtPIC1* and *AtIRT1* transporters along with the *AtFer1* gene were induced in response to GSH feeding while the expression was decreased in response to BSO treatment (Fig. 6B-F). The DTT feeding, however, failed to significantly alter the expression levels thus indicating that non-specific reducing condition was not sufficient for this regulation.

bioRxiv preprint doi: https://doi.org/10.1101/2021.05.09.443283; this version posted May 9, 2021. The copyright holder for this preprint (which was not certified by peer review) is the author/funder, who has granted bioRxiv a license to display the preprint in perpetuity. It is made available under aCC-BY-NC-ND 4.0 International license.

Since the *pad2-1* mutant is severely deficient in GSH content, we supplemented these mutant seedlings with exogenous GSH or DTT. It was observed that only GSH supplementation, and not DTT feeding, could compensate for its deficiency and resulted in an increased expression of the identified Fe responsive genes (Supplementary Fig. S3).

GSH modulated subcellular Fe homeostasis under Fe depleted condition

The Fe transporters *AtNRAMP3* and *AtNRAMP4* are vacuolar exporters for Fe while the *AtPIC1* is responsible for Fe influx into the chloroplast. In addition, *AtFer1* acts as a major Fe accumulator in the chloroplast. Since GSH was found to regulate the expression of all of these genes, it was hypothesized that GSH might be involved in modulating the subcellular Fe homeostasis under Fe deficient condition. To dissect this, the organellar Fe content was estimated from the *cad2-1* and *pad2-1* mutants along with the Col-0 plants under both control and DI conditions. It was observed that the chloroplast Fe content was significantly lower in the mutant lines as compared with the Col-0 plants under control as well as DI conditions (Fig. 7A). On the other hand, the vacuolar Fe content was lower in the mutants under control condition but higher under DI condition as compared with the Col-0 plants (Fig. 7B). This observation suggested that the mutant lines with depleted GSH levels failed to efficiently export the Fe from vacuoles and channelize them into the chloroplast under DI condition. The lower vacuolar Fe content in the mutants under control condition could be attributed to their lower *AtIRT1* expression and subsequent impaired Fe uptake.

GSH mediated regulation of Fe homeostasis involved GSNO

Since the association of GSH with GSNO is known in regulating Fe deficiency response, we were curious if this GSH mediated modulation of subcellular Fe homeostasis also involved GSNO. Therefore, the Col-0 and *pad2-1* plants were treated with GSH and GSNO in combination with their inhibitors and DI condition. The expression of *AtNRAMP3*, *AtNRAMP4*, *AtPIC1*, *AtIRT1* and *AtFER1* genes were then analyzed. When Col-0 plants were treated with GSH or GSNO under DI condition, stronger induction of the genes was observed as compared with DI condition alone (Fig. 8). Treating the plants with GSNO along with the GSH inhibitor, BSO under DI condition did not display this effect. Yet again, plants treated with GSH in combination with the nitrate reductase inhibitor, tungstate failed to induce the gene expression even under DI condition. These observations suggested that the GSH mediated regulation of the identified Fe responsive genes occurred in a GSNO-dependent manner. Similarly, in case of *pad2-1* mutant, the treatment with GSH or GSH-tungstate

bioRxiv preprint doi: https://doi.org/10.1101/2021.05.09.443283; this version posted May 9, 2021. The copyright holder for this preprint (which was not certified by peer review) is the author/funder, who has granted bioRxiv a license to display the preprint in perpetuity. It is made available under aCC-BY-NC-ND 4.0 International license.

combination under DI condition showed a similar trend like that of Col-0 plants. On contrary, GSNO treatment under DI condition failed to augment gene expression indicating that GSNO alone was not sufficient to trigger the expression of these genes under the GSH depleted condition.

GSH triggered promoter activation of the Fe responsive genes

Since GSH modulated the relative transcript abundance for the identified Fe responsive genes, it was assumed that a probable transcriptional regulation might be involved. To identify the mechanism of this regulation, transgenic lines harboring the *AtNRAMP3pro::GUS*, *AtNRAMP4pro::GUS*, *AtPIC1pro::GUS*, *AtFer1pro::GUS* and *AtIRT1pro::GUS* constructs were generated (Supplementary Fig. S4). A transgenic line harboring the *CaMV35S::GUS* construct was used as a negative control. The promoter activities in response to GSH and GSNO treatment were analyzed by histochemical GUS assay. The DI condition was used as a positive control for these treatments. The GUS activity in all the transgenic lines was found to be induced in response to both GSH and GSNO treatments which was also supported by the relative transcript abundance of the *GUS* gene (Fig. 9). On contrary, the GUS activity as well as its expression was unaltered in the *CaMV35S::GUS* containing negative control line. This observation strongly suggested that the GSH mediated regulation of these Fe responsive genes occurred via transcriptional activation.

GSH mediated transcriptional induction presumably involved S-nitrosylation of Fe-responsive TFs

Seventeen bHLH TFs are known to be involved in the transcriptional regulation of various Fe responsive genes (Gao *et al*., 2019; 2020). Among them, the *At*FIT, *At*bHLH38, *At*bHLH39, *At*bHLH100, and *At*bHLH101, were reported to be regulated directly or indirectly by GSNO (Meiser *at al*., 2011; Kailasham *et al*., 2018). This made us curious to check if the other known Fe responsive TFs were also regulated in a GSNO-dependent fashion. Therefore, the 12 known Fe responsive bHLH TFs, viz. *At*bHLH6, *At*bHLH11, *At*bHLH18, *At*bHLH19, *At*bHLH20, *At*bHLH25, *At*bHLH34, *At*bHLH47 (POPEYE), *At*bHLH104, *At*bHLH105, *At*bHLH115, and *At*bHLH121 were selected for this study and screened for probable *S*-nitrosylation sites using the GPS-SNO 1.0 software. Among them, *At*bHLH11, and *At*bHLH34 were found to contain 2 putative *S*-nitrosylation sites while *At*bHLH6, *At*bHLH18, *At*bHLH19, *At*bHLH105, and *At*bHLH115 contained 1 putative *S*-nitrosylation

bioRxiv preprint doi: https://doi.org/10.1101/2021.05.09.443283; this version posted May 9, 2021. The copyright holder for this preprint (which was not certified by peer review) is the author/funder, who has granted bioRxiv a license to display the preprint in perpetuity. It is made available under aCC-BY-NC-ND 4.0 International license.

site each (Supplementary Fig. S5; Supplementary Table S2). No sites were predicted in rest of the TFs. The enrichment analysis for the presence of *S*-nitrosylated cysteine residues in these TFs was performed as well (Supplementary Fig. S6). The bHLH TFs were reported to bind at the conserved E-box DNA binding (CANNTG) motif (Toledo-Ortiz *et al*., 2003). Therefore, the promoter regions of *AtNRAMP3*, *AtNRAMP4*, *AtPIC1*, *AtIRT1* and *AtFer1* genes were analyzed for the presence of this conserved CANNTG motif. Interestingly, the promoters of all these identified Fe responsive genes contained the conserved E-box motif indicating their probable interaction with the bHLH TFs (Supplementary Fig. S7). Together, these observations suggested that the GSH mediated regulation of the identified Fe responsive genes presumably involved transcriptional modulation via these *S*-nitrosylated bHLH TFs.

Discussion

In the last few decades the role of GSH in regulating multiple stress responses in plants was elaborately studied. Recently, emerging evidences suggested a positive role of GSH in mitigating Fe deficiency responses in plants (Koen *et al*., 2012; Ramirez *et al*., 2013). It was demonstrated that during Fe deficiency in *Arabidopsis*, the elevated level of GSH could significantly regulate different Fe responsive genes like *FRO*2, *IRT1*, *NAS4*, and *FIT1* to enhance Fe uptake and transport through roots (Koen *et al*., 2012). Subsequently, this GSH mediated regulation was found to occur in a GSNO dependent manner (Garcia *et al*., 2010, Shanmugam *et al*., 2015; Kailasam *et al*., 2018). However, the role of GSH in regulating subcellular Fe homeostasis in plants was not elucidated so far. In our previous study, comparative proteomic analysis of *pad2-1*, a GSH depleted mutant, revealed the down-accumulation of *At*Fer1 protein in shoot as compared with the Col-0 plants (Datta *et al*., 2015). This clue prompted us to investigate the role of GSH in regulating the expression of different Fe responsive genes in *Arabidopsis* shoot. Since ferritin is abundantly found in the chloroplast, we were also curious to identify any role of GSH in maintaining chloroplast Fe homeostasis. To begin with, we selected two GSH depleted mutants *cad2-1* and *pad2-1*, and analyzed their response under Fe limited conditions. Both the mutants displayed severe sensitivity to Fe deficiency as compared with the Col-0 plants with smaller rosette diameter and higher chlorosis level (Fig. 1). This observation was in line with the earlier study where Fe deficiency responses were found to be aggravated by reduced GSH content in *Arabidopsis* (Ramirez *et al*., 2013; Shanmugam *et al*. 2015). The next approach was to identify the Fe

bioRxiv preprint doi: https://doi.org/10.1101/2021.05.09.443283; this version posted May 9, 2021. The copyright holder for this preprint (which was not certified by peer review) is the author/funder, who has granted bioRxiv a license to display the preprint in perpetuity. It is made available under aCC-BY-NC-ND 4.0 International license.

transporters and homeostasis related genes that might be responsible for this observation. Out of the 32 Fe transporters analyzed, 2 vacuole Fe exporters, *AtNRAMP3* and *AtNRAMP4*, and a chloroplast Fe importer, *AtPIC1* were found to be significantly down-regulated in the mutants, while 2 chloroplast Fe exporters, *AtYSL1* and *AtYSL3* were up-regulated (Fig.3-5). Several Fe homeostasis related genes were analyzed as well among which *AtFer1* was found to be down-regulated in the mutants. Exogenously altered GSH levels also supported this observation (Fig 6).

The altered expression of these organellar Fe transporters suggested a possible role of GSH in modulating the subcellular Fe homeostasis under Fe limited condition. The vacuole, during Fe sufficient condition stores the excess amount of Fe to rescue the cell from Fe mediated oxidative damage. This stored Fe is released under Fe limited condition to mitigate Fe deficiency responses in plants (Morrissey and Guerinot, 2009). On contrary, *AtPIC1*, a chloroplast Fe importer, was found to be up-regulated during Fe deficiency to maintain the Fe homeostasis in chloroplast (Duy *et al*., 2005). In addition, *At*Fer1 was reported to act as Fe reservoir in chloroplast and to diminish the Fe deficiency responses (Briat *et al*., 2010). In a previous study, it was reported that *AtNRAMP3* and *AtNRAMP4* function as major vacuolar Fe exporters in germinating seeds where vacuolar reserve is the primary source of Fe (Bastow *et al*., 2018). Further, it was demonstrated that the Fe mobilization into chloroplast was limited when the vacuolar Fe could not be retrieved. The expression of *AtFer1* was also reported to be significantly reduced in the *nramp3nramp4* mutant with perturbed vacuolar Fe efflux. In this study, GSH was found to positively regulate the expression of *AtNRAMP3*, *AtNRAMP4*, *AtPIC1* and *AtFer1* genes. This made us inquisitive if GSH can help in channelizing the Fe retrieved from vacuoles into the chloroplast in shoot under Fe deficient conditions. We, therefore, analyzed the Fe content in the vacuoles and the chloroplasts in the GSH depleted mutants. Surprisingly, both the vacuolar and chloroplast Fe contents were found to be lower in the mutants under Fe sufficient condition (Fig. 7). This lower Fe accumulation in the mutants can be attributed to their impaired Fe uptake due to reduced *AtIRT1* expression in the roots. On contrary, the vacuolar Fe content was found to be higher in the mutants while the chloroplast Fe content remained lower under DI condition. This observation strongly suggested that the GSH depleted mutants failed to efficiently retrieve the vacuolar Fe under DI condition and channelize them into the chloroplast.

bioRxiv preprint doi: https://doi.org/10.1101/2021.05.09.443283; this version posted May 9, 2021. The copyright holder for this preprint (which was not certified by peer review) is the author/funder, who has granted bioRxiv a license to display the preprint in perpetuity. It is made available under aCC-BY-NC-ND 4.0 International license.

GSH combines with NO leading to the formation of GSNO which acts as an important signaling intermediate. Earlier, GSNO was reported to act as a key modulator of Fe responsive genes in Arabidopsis (Koen *et al*., 2012; Shanmugam *et al*. 2015; Kailasam *et al*., 2018). This made us interested to dissect the role of GSNO in regulating these Fe responsive genes. The Col-0 and *pad2-1* plants, when fed with GSH or GSNO under DI condition showed marked increment in the expression of all 5 genes (Fig 8). On contrary, feeding the plants with GSNO/BSO combination under DI condition, did not display this augmented expression pattern as compared with the DI condition alone. Again, no induction in gene expression was observed in case of combined GSH/tungstate treatment even under DI condition. These observations suggested that GSH regulated the subcellular Fe homeostasis via a GSNO mediated pathway.

The next pertinent question was how this GSH-GSNO module induced the expression of these genes. To dissect this mechanism, 5 different transgenic lines harbouring *AtNRAMP3pro::GUS*, *AtNRAMP4pro::GUS*, *AtPIC1pro::GUS*, *AtFer1pro::GUS*, and *AtIRT1pro::GUS* constructs were generated and the transgenic plants were used for promoter analysis. Interestingly, the histochemical GUS assay confirmed that all the 5 promoters were activated in response to GSH or GSNO treatments. This strongly indicated that the GSH-GSNO module regulated the Fe responsive genes via transcriptional activation. Since neither GSH nor GSNO can directly bind to these promoters, this transcriptional activation presumably involved one or more TFs. Earlier reports have identified 17 bHLH TFs that are involved in regulating various Fe responsive genes in *Arabidopsis* (Yuan *et al*., 2008; Gao *et al*., 2019; 2020). Among them, *At*FIT1 (bHLH29, clade IIIa) and the clade Ib bHLH factors (bHLH38, bHLH39, bHLH100, bHLH101) were reported to regulate two crucial Fe responsive genes, *AtIRT1* and *AtFRO2* (Colangelo and Guerinot, 2004; Yuan *et al*., 2008). Further, these TFs were found to be regulated directly or indirectly by GSNO (Darbani *et al*., 2013; Kailasam *et al*., 2018). This GSNO mediated regulation often involved *S*-nitrosylation of the TFs (Darbani *et al*., 2013). We were curious if the rest of the 12 bHLH TFs could be regulated by GSNO as well and analyzed for the presence of putative *S*-nitrosylation sites. Seven out of these 12 TFs were found to contain at least one putative *S*-nitrosylation sites supporting the hypothesis for a GSNO-mediated regulation (Supplementary Fig. S5-6). Moreover, the identified Fe responsive genes, viz. *AtNRAMP3*, *AtNRAMP4*, *AtPIC1*, *AtIRT1* and *AtFer1* were found to contain conserved E-box motifs in their promoter regions

bioRxiv preprint doi: https://doi.org/10.1101/2021.05.09.443283; this version posted May 9, 2021. The copyright holder for this preprint (which was not certified by peer review) is the author/funder, who has granted bioRxiv a license to display the preprint in perpetuity. It is made available under aCC-BY-NC-ND 4.0 International license.

indicating the probable transcriptional regulation via the *S*-nitrosylated bHLH TFs (Supplementary Fig. S7). This remains an open area for in depth analysis in the future.

In summary, it can be postulated that during Fe deficiency the accumulation of GSH in cells can activate the vacuolar Fe exporters like *AtNRAMP3* and *AtNRAMP4* to facilitate Fe export from the vacuolar reserve. On the other hand, GSH was found to trigger the expression of chloroplast Fe importer, *AtPIC1* and Fe responsive gene *AtFer1* to maintain chloroplast Fe content during Fe deficiency in plants (Fig. 10). This regulation involved GSH-GSNO mediated transcriptional activation of these genes presumably via *S*-nitrosylation of different Fe responsive bHLH TFs.

Supplementary data

Fig. S1. Expression of *AtIRT1* gene in Col-0 shoot under DI condition. 7 d old MS grown seedlings were transferred to DI medium and samples were collected after 0 d, 2 d, 5 d, 7 d, and 10 d of treatment.

Fig. S2. Perls-DAB staining of Col-0, *cad2-1* and *pad2-1* plants grown under MS condition.

Fig. S3. Response of *pad2-1* plants to exogenous GSH and DTT treatments. (A) Total GSH content. (B-F) Relative transcript abundance of the identified Fe responsive genes.

Fig. S4. Screening of transgenic lines harbouring (A) *CaMV35S::GUS*, (B) *AtPIC1pro::GUS*, (C) *AtNRAMP3pro::GUS*, (D) *AtIRT1pro::GUS*, (E) *AtFer1pro::GUS*, and (F) *AtNRAMP4pro::GUS* constructs.

Fig. S5. Prediction of putative *S*-nitrosylation sites in different Fe responsive bHLH TFs using GPS-SNO 1.0 Software and Centrimo 5.3.3 web server.

Fig. S6. Enrichment analysis for the presence of putative *S*-nitrosylation cysteine residues in different Fe responsive bHLH TFs.

Fig. S7. *In silico* promoter analysis of the identified Fe responsive genes for the presence of conserved E-box motif.

Table S1. List of primers used.

Table S2. Prediction of putative *S*-nitrosylation sites using GPS-SNO 1.0 software.

Acknowledgement

bioRxiv preprint doi: https://doi.org/10.1101/2021.05.09.443283; this version posted May 9, 2021. The copyright holder for this preprint (which was not certified by peer review) is the author/funder, who has granted bioRxiv a license to display the preprint in perpetuity. It is made available under aCC-BY-NC-ND 4.0 International license.

This work has been supported by the Science and Engineering Research Board, Government of India [ECR/2017/000231] and Start up Grant, University Grant Commission, Government of India, India [F30-363/2017(BSR)]. We thank the central instrumentation facility of the Department of Botany, University of Calcutta and Department of Botany, Dr A. P. J. Abdul Kalam Government College. We thank Prof. Manoj Prasad, Staff Scientist VII, NIPGR, New Delhi for providing us the pCAMBIA1304 vector.

Author Contributions

RD and SP conceived and designed the research plan; RS raised the transgenic lines, performed expression analysis, feeding experiments and GUS assay; SG standardized the plant growth and stress treatments, PK performed biochemical experiments, SS prepared the constructs; CR helped in maintaining the transgenic lines, DS performed *in silico* analysis; RD and SP analyzed the data and prepared the manuscript.

References

Anderson. 1985. Determination of glutathione and glutathione disulfide in biological samples. Methods in Enzymology **113,** 548- 555.

Bailey TL, Bodén M, Buske FA, Frith M, Grant CE, Clementi L, Ren J, Li WW, Noble WS. 2009. MEME SUITE: tools for motif discovery and searching. Nucleic Acids Research **37,** 202-208.

Bailey TL, Machanick P. 2012.Inferring direct DNA binding from ChIP-seq. Nucleic Acids Research **40**,128.

Ball L, Accotto G, Bechtold U, Creissen G, Funck, D, Jimenez A, Kular B, Leyland N, Mejia-Carranza J, Reynolds H, Karpinski S, Mullineaux PM. 2004.Evidence for a direct link between glutathione biosynthesis and stress defense gene expression in Arabidopsis. Plant Cell **16,** 2448–2262.

Bashandy T, Guilleminot J, Vernoux T, Caparros-Ruiz D, Ljung, K, Meyer Y, Reichheld JP. 2010. Interplay between the NADP-linked thioredoxin and glutathione systems in Arabidopsis auxin signaling. Plant Cell **22,** 376–391.

bioRxiv preprint doi: https://doi.org/10.1101/2021.05.09.443283; this version posted May 9, 2021. The copyright holder for this preprint (which was not certified by peer review) is the author/funder, who has granted bioRxiv a license to display the preprint in perpetuity. It is made available under aCC-BY-NC-ND 4.0 International license.

Bastow EL, Vanesa S, Torre G, Maclean AE, Merlot S, Thomine S, Balk J. 2018. Vacuolar Iron Stores Gated by NRAMP3 and NRAMP4 are the Primary Source of Iron in Germinating Seeds. Plant Physiology **177**, 1267–1276.

Briat JF, Ravet K, Arnaud N, Duc C, Boucherez J, Touraine B, Cellier F, Gaymard F. 2010. New insights into ferritin synthesis and function highlight a link between iron homeostasis and oxidative stress in plants. Annals of Botany **105**, 811–822.

Briat, JF, Dubos C, Gaymard F. 2015. Iron nutrition, biomass production, and plant product quality. Trends in Plant Science **20,** 33–40.

Cairns N, Pasternak M, Wachter A, Cobbett C, Meyer A. 2006. Maturation of Arabidopsis seeds is dependent on glutathione biosynthesis within the embryo. Plant Physiology **141,** 446–455.

Chen WW, Yang JL, Qin C, Jin CW, Mo JH, Ye T, Zheng SJ. 2010. Nitric oxide acts downstream of auxin to trigger root ferric□chelate reductase activity in response to iron deficiency in Arabidopsis. Plant Physiology **154,** 810– 819.

Chu HH, Chiecko J, Punshon T, Lanzirotti A, Lahner B, Salt DE, Walker EL. 2010. Successful reproduction requires the function of Arabidopsis YELLOW STRIPE-LIKE1 and YELLOW STRIPE-LIKE3 metal-nicotianamine transporters in both vegetative and reproductive structures. Plant Physiology **154**, 197–210.

Clemens S, Kim E, Neumann D, Schroeder J. 1999.Tolerance to toxic metals by a gene family of phytochelatin synthases from plants and yeast. EMBO Journal **18,** 3325–3333.

Clough, SJ, Bent AF. 1998. Floral dip: a simplified method for *Agrobacterium*-mediated transformation of *Arabidopsis thaliana*. Plant Journal **16,** 735–743.

Colangelo EP, Guerinot, ML. 2004. The essential basic helix□loop□helix protein FIT1 is required for the iron deficiency response. Plant Cell **16,** 3400– 3412.

Curie C, Alonso JM, Marie LE , Ecker JR, Briat JF. 2000. Involvement of NRAMP1 from Arabidopsis thaliana in iron transport. Biochemical Journal **347,** 749–755.

Darbani B, Briat JF, Holm PB, Husted S, Noeparvar S, Borg S. 2013.Dissecting plant iron homeostasis under short and long-term iron fluctuations. Biotechnology Advances **31,** 1292–1307.

bioRxiv preprint doi: https://doi.org/10.1101/2021.05.09.443283; this version posted May 9, 2021. The copyright holder for this preprint (which was not certified by peer review) is the author/funder, who has granted bioRxiv a license to display the preprint in perpetuity. It is made available under aCC-BY-NC-ND 4.0 International license.

Datta R, Kumar D, Sultana A, Hazra S, Bhattacharyya D, Chattopadhyay S. 2015. Glutathione Regulates 1-Aminocyclopropane-1-Carboxylate Synthase Transcription via WRKY33 and 1-Aminocyclopropane-1-Carboxylate Oxidase by Modulating Messenger RNA Stability to Induce Ethylene Synthesis during Stress. Plant Physiology **169,** 2963–2981.

Datta R, Chattopadhyay S. 2015. Changes in the proteome of pad2.1, a glutathione depleted Arabidopsis mutant, during *Pseudomonas syringae* infection. Journal of Proteomics **126,** 82–93.

Duy D, Gerhard W, Meda AR, Wirén NV, Soll J, Philippar K. 2007. PIC1, an Ancient Permease in Arabidopsis Chloroplasts, Mediates Iron Transport. Plant Cell **19,** 986–1006.

Eroglu S, Meier B, Wirén NV, Peiter E. 2016. The Vacuolar Manganese Transporter MTP8 Determines Tolerance to Iron Deficiency-Induced Chlorosis in Arabidopsis. Plant Physiology **170**, 1030–1045.

Foyer CH, Halliwell B. 1976. The presence of glutathione and glutathione reductase in chloroplasts: A proposed role in ascorbic acid metabolism. Planta **133,** 21–25.

Frottin F, Espagne C, Traverso J, Mauve C, Valot B, Lelarge-Trouverie C, Zivy M, Noctor G, Meinnel T, Giglione C. 2009. Cotranslational proteolysis dominates glutathione homeostasis to support proper growth and development. Plant Cell **21,** 3296–3314.

Gao F, Robe K, Bettembourg M, Navarro N, Rofidal V, Santoni V, Gaymard F, Florence V, Roschzttardtz H, Izquierdo E, Dubos C. 2020. The Transcription Factor bHLH121 Interacts with bHLH105 (ILR3) and Its Closest Homologs to Regulate Iron Homeostasis in Arabidopsis. Plant Cell **32,** 508–524.

Gao F, Robe K, Gaymard F, Izquierdo E, Dubos B. 2019. The Transcriptional control of iron homeostasis in plants: a tale of bHLH transcription factors? Frontiers in Plant Science **10,** 1-8.

García MJ, Lucena C, Romera FJ, Alcántara E, Vicente P. 2010. Ethylene and nitric oxide involvement in the up-regulation of key genes related to iron acquisition and homeostasis in Arabidopsis. Journal of Experimental Botany **61,** 3885–3899.

bioRxiv preprint doi: https://doi.org/10.1101/2021.05.09.443283; this version posted May 9, 2021. The copyright holder for this preprint (which was not certified by peer review) is the author/funder, who has granted bioRxiv a license to display the preprint in perpetuity. It is made available under aCC-BY-NC-ND 4.0 International license.

Ghanta S, Bhattacharyya D, Sinha, R, Banerjee A, Chattopadhyay S. 2011. Nicotiana tabacum overexpressing γ-eCS exhibits biotic stress tolerance likely through NPR1-dependent salicylic acid-mediated pathway. Planta **233,** 895–910.

Ghanta S, Datta R, Bhattacharyya D, Sinha R, Kumar D, Hazra S, Bose Mazumdar A, Chattopadhyay S. 2014.Multistep involvement of glutathione with salicylic acid and ethylene to combat environmental stress. Journal of Plant Physiology **171,** 940-950.

Glazebrook J, Ausubel FM. 1994.Isolation of phytoalexin-deficient mutants of Arabidopsis thaliana and characterization of their interactions with bacterial pathogens. Proceedings of the National Academy of Sciences, USA **91,** 8955– 8959.

Glazebrook J, Zook M, Mert F, Kagan I, Rogers EE, Crute IR, Holub EB, Hammerschmidt R, Ausubel FM. 1997. Phytoalexin-deficient mutants of Arabidopsis reveal that PAD4 encodes a regulatory factor and that four PAD genes contribute to downy mildew resistance. Genetics **146,** 381–392.

Grill E, Löffler S, Winnacker E, Zenk M. 1989. Phytochelatins, the heavy-metal-binding peptides of plants, are synthesized from glutathione by a specific gamma-glutamylcysteine dipeptidyl transpeptidase (phytochelatin synthase). Proceedings of the National Academy of Sciences, USA **86,** 6838–6842.

Han Y, Chaouch S, Mhamdi A, Queval G, Zechmann B, Noctor G. 2013. Functional analysis of Arabidopsis mutants points to novel roles for glutathione in coupling H_2O_2 to activation of salicylic acid accumulation and signaling. Antioxidamts & Redox Signaling **18,** 2106–2121.

Hider RC, Kong XL. 2011. Glutathione: A key component of the cytoplasmic labile iron pool. Biometals **24,** 1179–1187.

Jefferson RA, Kavangh TA, Bevan MW. 1987. Gus fusions: β-glucuronidase as a sensitive and versatile gene fusion marker in higher plants. EMBO Journal **6,** 3901-3907.

Jeong J, Connolly EL. 2009. Iron uptake mechanisms in plants: functions of the FRO family of ferric reductases. Plant Science **176,** 709–714.

Jiang SL, Wu JG, Feng Y, Yang XE, Shi CH. 2007.Correlation analysis of mineral element contents and quality traits in milled rice (Oryza sativa L.). Journal of Agricultural and Food Chemisty **55,** 9608–9613.

bioRxiv preprint doi: https://doi.org/10.1101/2021.05.09.443283; this version posted May 9, 2021. The copyright holder for this preprint (which was not certified by peer review) is the author/funder, who has granted bioRxiv a license to display the preprint in perpetuity. It is made available under aCC-BY-NC-ND 4.0 International license.

Jobe T, Sung D, Akmakjian G, Pham A, Komives E, Mendoza Cózatl DG Schroeder JI. 2012. Feedback inhibition by thiols outranks glutathione depletion: A luciferase-based screen reveals glutathione-deficient γ-eCS and glutathione synthetase mutants impaired in cadmium-induced sulfate assimilation. Plant Journal **70,** 783–795.

Kailasam S, Wang Y, Lo JC, Chang HF, Yeh KC. 2018. S-nitrosoglutathione works downstream of nitric oxide to mediate iron deficiency signaling in Arabidopsis. Plant Journal **94,** 157–168.

Kim SA, Punshon T, Lanzirotti A, Li L, Alonso JM, Ecker JR, Kaplan J, Mary L. 2006. Localization of iron in Arabidopsis seed requires the vacuolar membrane transporter VIT1. Science **314,** 1295-1298.

Kleffmann T, Russenberger D, Zychlinski A, Christopher W, Sjolander K, Gruissem W, Baginsky S. 2004. The Arabidopsis thaliana chloroplast proteome reveals pathway abundance and novel protein functions. Current Biology **14,** 354–362.

Koen E, Szymańska K, Klinguer A, Dobrowolska G, Besson-Bard A, Wendehenne D. 2012. Nitric oxide and glutathione impact the expression of iron uptake- and iron transport-related genes as well as the content of metals in A. thaliana plants grown under iron deficiency. Plant Signaling and Behavior **7,** 1246-1250.

Kumar C, A Igbaria, D'Autreaux B , Planson AG, Junot C, Godat E, Bachhawat AK, Moisan AD, Toledano MB. 2011. Glutathione revisited: a vital function in iron metabolism and ancillary role in thiol-redox control. EMBO Journal **30,** 2044-2056.

Lanquar V, Lelievre F, Bolte S, Hames C, Alcon C, Neumann D, Vansuyt G, Curie C, Schroder A, Kramer U. 2005. Mobilization of vacuolar iron by Atnramp3 and Atnramp4 is essential for seed germination on low iron. EMBO Journal **24,** 4041–4051.

Lichtenthaler HK. 1987. Chlorophylls and carotenoids: pigments of photosynthetic biomembranes. Methods Enzymology **148,** 350–382.

Meiser J, Lingam S, Bauer P. 2011. Posttranslational regulation of iron deficiency basic-helix-loop-helix transcription factor FIT is affected by iron and nitric oxide. Plant Physiology **157,** 2154–2166.

Morrissey J, Guerinot ML. 2009. Iron uptake and transport in plants: The good, the bad, and the ionome. Chemical Review **10,** 4553–4567.

bioRxiv preprint doi: https://doi.org/10.1101/2021.05.09.443283; this version posted May 9, 2021. The copyright holder for this preprint (which was not certified by peer review) is the author/funder, who has granted bioRxiv a license to display the preprint in perpetuity. It is made available under aCC-BY-NC-ND 4.0 International license.

Murashige T, Skoog F. 1962. A revised medium for rapid growth and bio assays with tobacco tissue cultures. Physiologia Plantarum **15,** 473-497.

Parisy V, Poinssot B, Owsianowski L, Buchala A, Glazebrook J, Mauch F. 2007. Identification of PAD2 as a gamma-glutamylcysteine synthetase highlights the importance of glutathione in disease resistance of Arabidopsis. Plant Journal **49,** 159–172.

Qiu B, Zeng F, Cai S, Wu X, Haider S, Wu F, Zhang G. 2013. Alleviation of chromium toxicity in rice seedlings by applying exogenous glutathione. Journal of Plant Physiology **170,** 772–779.

Queval G, Thominet D, Vanacker H, Miginiac-Maslow M, Gakiere B, Noctor G. 2009. H_2O_2-activated upregulation of glutathione in Arabidopsis involves induction of genes encoding enzymes involved in cysteine synthesis in the chloroplast. Molecular Plant **2,** 344–356.

Ramirez L, Bartoli CG, Lamattina L. 2013. Glutathione and ascorbic acid protect Arabidopsis plants against detrimental effects of iron deficiency. Journal of Experimental Botany **64,** 3169-3178.

Ramirez L, Simontacchi M, Murgia I. Zabaleta E. Lamattina L. 2011. Nitric oxide, nitrosyl iron complexes, ferritin and frataxin: a well equipped team to preserve plant iron homeostasis. Plant Science **181,** 582– 592.

Reichheld JP, Khafif M, Riondet C, Droux M, Bonnard G, Meyer Y. 2007. Inactivation of thioredoxin reductases reveals a complex interplay between thioredoxin and glutathione pathways in Arabidopsis development. Plant Cell **19,** 1851–1865.

Requejo R, Tena M. 2012. Influence of glutathione chemical effectors in the response of maize to arsenic exposure. Journal of Plant Physiology **169,** 649–656.

Robinson NJ, Procter CM, Connolly EL, Guerinot ML. 1999. A ferric-chelate reductase for iron uptake from soils. Nature **397**, 694–697.

Roschzttardtz H, Conéjéro G, Curie C, Mari S. 2009. Identification of the endodermal vacuole as the iron storage compartment in the Arabidopsis embryo. Plant Physiology **151,** 1329–1338.

bioRxiv preprint doi: https://doi.org/10.1101/2021.05.09.443283; this version posted May 9, 2021. The copyright holder for this preprint (which was not certified by peer review) is the author/funder, who has granted bioRxiv a license to display the preprint in perpetuity. It is made available under aCC-BY-NC-ND 4.0 International license.

Schützendübel A, Schwanz, P, Teichmann T, Gross K, Rosemarie LH, Godbold D, Polle A. 2001. Cadmium-induced changes in antioxidative systems, hydrogen peroxide content, and differentiation in Scots pine roots. Plant Physiology **127,** 887–898.

Shanmugam V, Tsednee M, Yeh KC. 2012. ZINC TOLERANCE INDUCED BY IRON 1 reveals the importance of glutathione in the cross□homeostasis between zinc and iron in Arabidopsis thaliana. Plant Journal **69,** 1006–1017.

Shanmugam V, Wang YW, Tsednee M, Karunakaran K, Yeh KC. 2015. Glutathione plays an essential role in nitric oxide□mediated iron□deficiency signaling and iron□deficiency tolerance in Arabidopsis. Plant Journal **84,** 464-477.

Shimoni SE, Hassidim M, Yuval-Neah N, Keren N. 2010. Disruption of Nap14, a plastid□localized non□intrinsic ABC protein in Arabidopsis thaliana results in the over□accumulation of transition metals and in aberrant chloroplast structures. Plant Cell & Environment **33,** 1029–1038.

Taylor NL, Millar AH. 2016. Isolation of Plant Organelles and Structures. Methods in Molecular Biology **1511,** 113-118.

Thomine S, Lelievre F, Debarbieux E, Schroeder JI, Brygoo HB. 2003. AtNRAMP3, a multispecific vacuolar metal transporter involved in plant responses to iron deficiency. Plant Journal **34,** 685-695.

Toledo-Ortiz G, Huq E, Quail PH. 2003.The Arabidopsis basic/helix-loop-helix transcription factor family. Plant Cell **15,** 1749–1770.

Vatamaniuk OK, Mari S, Lu YP, Rea PA. 1999. AtPCS1, a phytochelatin synthase from Arabidopsis: Isolation and in vitro reconstitution. Proceedings of the National Academy of Sciences, USA **96,** 7110–7115.

Vernoux T, Wilson R, Seeley K, Reichheld J, Muroy S, Brown S, Maughan SC, Cobbett SC, Montagu MV, Inzé D, May MJ, Sung Z. 2000. The ROOT MERISTEMLESS1/CADMIUM SENSITIVE2 gene defines a glutathione-dependent pathway involved in initiation and maintenance of cell division during postembryonic root development. Plant Cell **12,** 97–110.

bioRxiv preprint doi: https://doi.org/10.1101/2021.05.09.443283; this version posted May 9, 2021. The copyright holder for this preprint (which was not certified by peer review) is the author/funder, who has granted bioRxiv a license to display the preprint in perpetuity. It is made available under aCC-BY-NC-ND 4.0 International license.

Vert G, Grotz N, Dédaldéchamp F, Gaymard F, Guerino ML, Briat JF, Curie C. 2002. IRT1, an Arabidopsis Transporter Essential for Iron Uptake from the Soil and for Plant Growth. Plant Cell **22,** 376–391.

Waters BM, Chu HH, DiDonato RJ, Roberts LA, Eisley RB, Lahner B, Salt DE, Walker EL. 2006. Mutations in Arabidopsis yellow stripe-like1 and yellow stripe-like3 reveal their roles in metal ion homeostasis and loading of metal ions in seeds. Plant Physiology 141, 1446–1458.

Xue Y, Liu Z, Gao X, Jin C, Wen L, Yao X, Ren J. 2010. GPS-SNO: Computational prediction of protein *S*-nitrosylation sites with a modified GPS algorithm. Plos One **5,** e11290.

Yuan Y, Wu H, Wang N, Li, J, Zhao W, Du J, Wang D, Ling HQ. 2008. FIT interacts with AtbHLH38 and AtbHLH39 in regulating iron uptake gene expression for iron homeostasis in Arabidopsis. Cell Research **18**, 385–397.

Zeng F, Qiu B, Wu X, Niu S, Wu F, Zhang G. 2012. Glutathione-mediated alleviation of chromium toxicity in rice plants. Biological Trace Element Research **148,** 255–263.

bioRxiv preprint doi: https://doi.org/10.1101/2021.05.09.443283; this version posted May 9, 2021. The copyright holder for this preprint (which was not certified by peer review) is the author/funder, who has granted bioRxiv a license to display the preprint in perpetuity. It is made available under aCC-BY-NC-ND 4.0 International license.

Figure Legends

Fig. 1. Morphological response of Col-0, *cad2-1* and *pad2-1* plants in response to Fe deficient conditions. 7 d old MS grown seedlings were exposed to MI and DI condition for 7 d and morphological parameters were recorded. (A) Shoot and (B) root morphology, (C) Rosette diameter, (D) primary root length, (E) Lateral root density, and (F) Total chlorophyll content. Results were represented as mean±SEM (n=3). Statistical differences between the Col-0, *cad2-1* and *pad2-1* were denoted by asterisks at P<0.05 (*), P<0.01 (**), P< 0.001 (***), and P< 0.0001 (****).

Fig. 2. Biochemical analyses of of Col-0, *cad2-1* and *pad2-1* plants in response to Fe deficient conditions. 7 d old MS grown seedlings were exposed to MI and DI condition for 7 d and biochemical parameters were recorded. (A) Shoot Fe content, (B) Shoot total GSH content, (C) Shoot GSH:GSSG ratio, (D) Root Fe content, (E) Root total GSH content, and (F) Root GSH:GSSG ratio. Results were represented as mean±SEM (n=3). Statistical differences between the Col-0, *cad2-1* and *pad2-1* were denoted by asterisks at P<0.05 (*), P< 0.001 (***), and P< 0.0001 (****).

Fig. 3. Expression analysis of different Fe transporters in Col-0, *cad2-1* and *pad2-1* plants. 14 d old MS grown plants were used for qRT-PCR analysis to analyse the relative transcript abundance of various Fe transporter genes from shoot tissue. Results were represented as mean±SEM (n=3). Statistical differences between the Col-0, *cad2-1* and *pad2-1* were denoted by asterisks at P<0.05 (*), and P< 0.01 (**).

Fig. 4. Expression analysis of different Fe homeostasis related genes in Col-0, *cad2-1* and *pad2-1* plants. 14 d old MS grown plants were used for qRT-PCR analysis to analyse the relative transcript abundance of various Fe homeostasis related genes from shoot tissue. Results were represented as mean±SEM (n=3). Statistical differences between the Col-0, *cad2-1* and *pad2-1* were denoted by asterisks at P<0.05 (*), and P< 0.01 (**).

Fig. 5. Expression analysis of the identified Fe responsive genes in Col-0, *cad2-1* and *pad2-1* plants under DI condition. 7 d old MS grown seedlings were exposed to DI condition for 7 d and were used for qRT-PCR analysis. Results were represented as mean±SEM (n=3). Statistical differences between Col-0, *cad2-1* and *pad2-1* were denoted by asterisks at P<0.05 (*), P< 0.01 (**), and P<0.0001 (****).

bioRxiv preprint doi: https://doi.org/10.1101/2021.05.09.443283; this version posted May 9, 2021. The copyright holder for this preprint (which was not certified by peer review) is the author/funder, who has granted bioRxiv a license to display the preprint in perpetuity. It is made available under aCC-BY-NC-ND 4.0 International license.

Fig. 6. Expression analysis of the identified Fe responsive genes in Col-0 plants in response to exogenously altered GSH level. 15 d old MS grown plants were treated with 100 μM GSH, or 1 mM BSO, or 5 mM DTT solutions. Control plants were maintained in half strength MS medium for the entire duration. Shoot samples collected from each set were used for qRT-PCR analysis. Results were represented as mean±SEM (n=3). Statistical differences between the control, +GSH, +BSO and +DTT plants were denoted by asterisks at P<0.05 (*), P<0.01 (**), P< 0.001 (***), and P< 0.0001 (****).

Fig. 7. Estimation of organellar Fe content from Col-0, *cad2-1* and *pad2-1* plants under MS and DI conditions. 7 d old MS grown seedlings were exposed to DI condition for 7 d. Control plants were maintained in the MS medium for the entire period. Chloroplasts and vacuoles were isolated from the samples and used for Fe content estimation. (A) Chloroplast Fe content, and (B) Vacuolar Fe content. Results were represented as mean±SEM (n=3). Statistical differences between Col-0, *cad2-1* and *pad2-1* were denoted by asterisks at P<0.01 (**), P< 0.001 (***), and P< 0.0001 (****).

Fig. 8. **Expression analysis of the identified Fe responsive genes in Col-0 and *pad2-1* plants in response to chemical treatments.** 7 d old seedlings were transferred to DI condition for 7 d with or without GSH or GSNO or GSH/tungstate combination or GSNO/BSO combination. Control plants were maintained in half strength MS medium for the entire duration. Shoot samples collected from each set were used for qRT-PCR analysis. Results were represented as mean±SEM (n=3). Statistical differences between the different set of treatments were denoted by asterisks at P<0.05 (*), P<0.01 (**), P< 0.001 (***), and P< 0.0001 (****).

Fig. 9. Promoter analysis of the identified Fe responsive genes. The seedlings of different transgenic lines were exposed to GSH or GSNO treatment and used to analyse their promoter activity by histochemical GUS assay and qRT-PCR analysis for *GUS* gene expression. The DI condition was used as a positive control. (A) *proNRAMP3* (harbouring *AtNRAMP3pro::GUS* construct), (B) *proNRAMP4* (harbouring *AtNRAMP4pro::GUS* construct), (C) *proFer1* (harbouring *AtFer1pro::GUS* construct), (D) *proPIC1* (harbouring *AtPIC1pro::GUS* construct), and (E) *proIRT1* (harbouring *AtIRT1pro::GUS* construct). A control transgenic line harbouring the *CaMV35S::GUS* construct was used as a negative control (E). Representative images of histochemical GUS staining were presented. The experiment was independently repeated thrice. For relative transcript abundance, results were

bioRxiv preprint doi: https://doi.org/10.1101/2021.05.09.443283; this version posted May 9, 2021. The copyright holder for this preprint (which was not certified by peer review) is the author/funder, who has granted bioRxiv a license to display the preprint in perpetuity. It is made available under aCC-BY-NC-ND 4.0 International license.

represented as mean±SEM (n=3). Statistical differences between the MS, DI, +GSH, and +GSNO plants were denoted by asterisks at P<0.05 (*), P<0.01 (**), P< 0.001 (***), and P< 0.0001 (****).

Fig. 10. Model for GSH mediated regulation of subcellular Fe homeostasis under Fe limited condition. Fe deficiency leads to the accumulation of GSH in cells. GSH then activates the vacuolar Fe exporters, *At*NRAMP3 and *At*NRAMP4, to facilitate release of Fe from the vacuolar reserve. GSH also induces the chloroplast Fe importer, *At*PIC1, along with *At*Fer1 which aids in channelizing the released Fe into the chloroplast. This GSH mediated modulation involves transcriptional induction via GSNO, presumably by *S*-nitrosylation of different Fe responsive bHLH TFs.

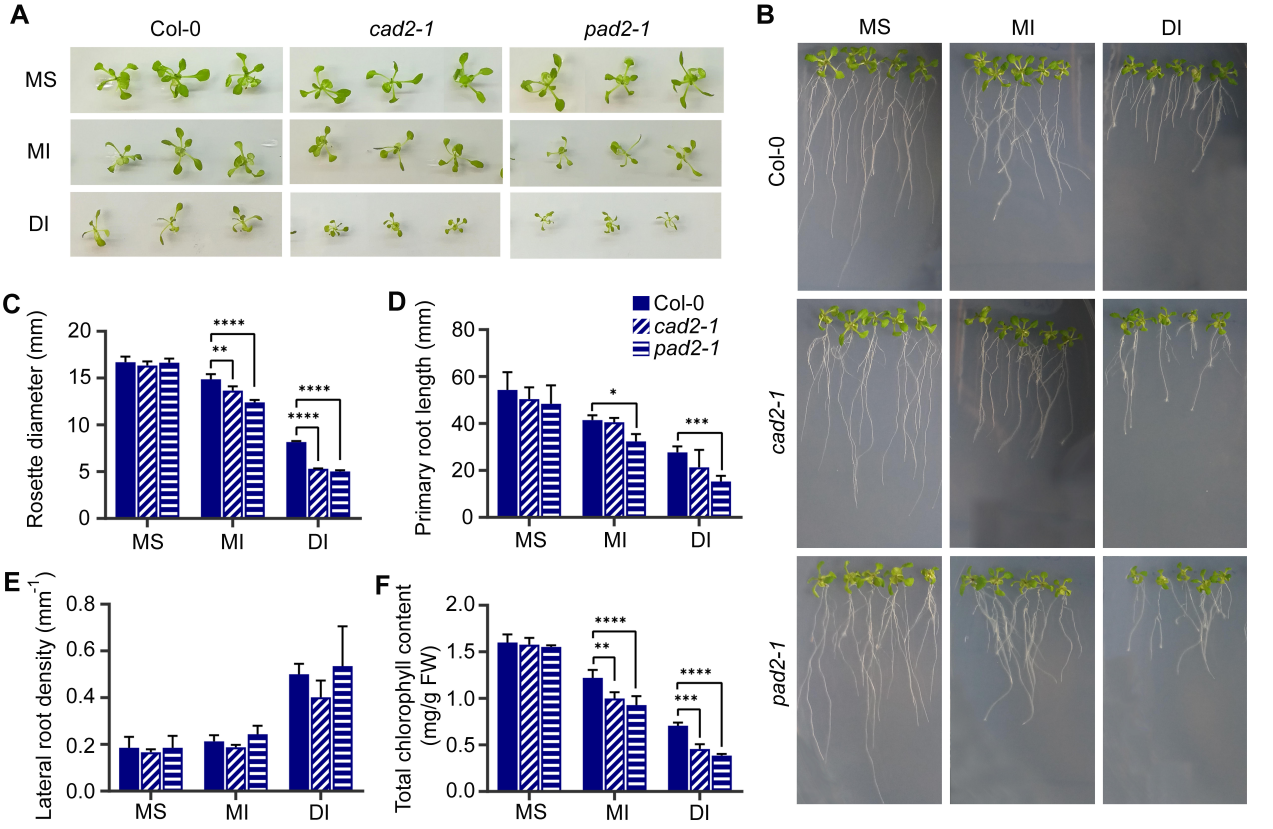
A
Col-0
cad2-1
pad2-1
MS
MI
DI
B
MS
MI
DI
Col-0
cad2-1
pad2-1
C
Rosette diameter (mm)
20
15
10
5
0
****
**
****
****
MS
MI
DI
D
Primary root length (mm)
80
60
40
20
0
Col-0
cad2-1
pad2-1
*
***
MS
MI
DI
E
Lateral root density (mm-1)
0.8
0.6
0.4
0.2
0.0
MS
MI
DI
F
Total chlorophyll content (mg/g FW)
2.0
1.5
1.0
0.5
0.0
****
**
****
***
MS
MI
DI

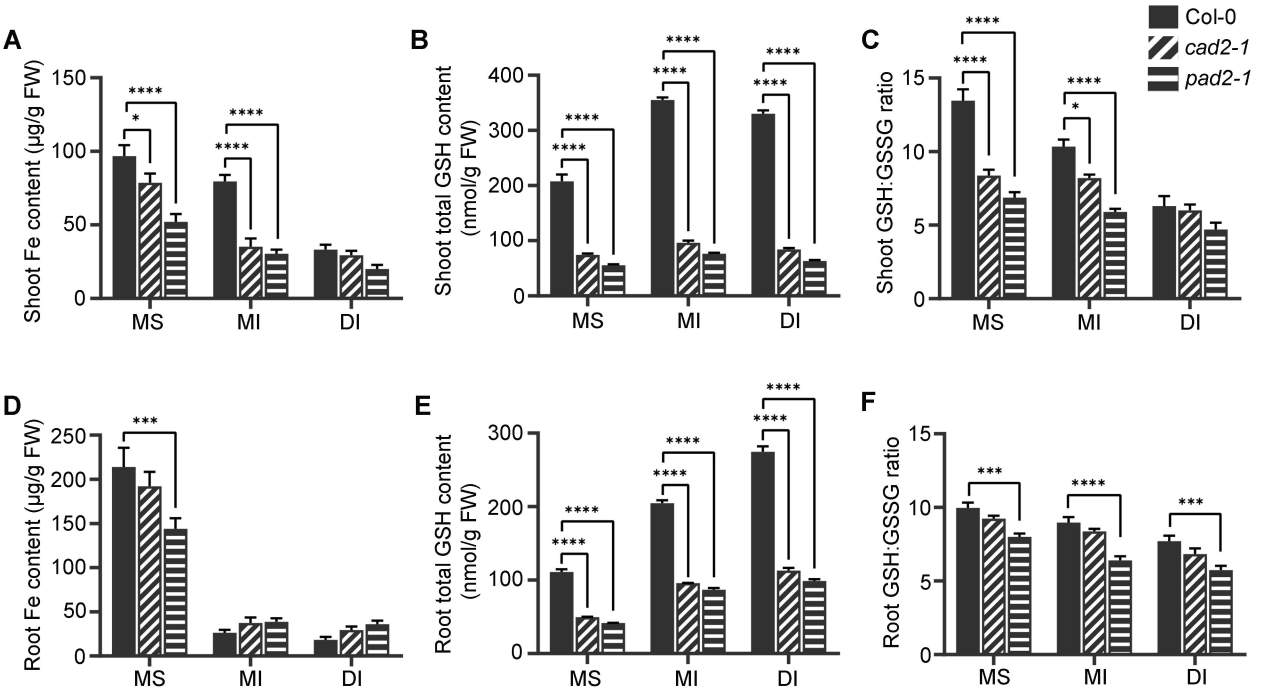
A
Shoot Fe content (µg/g FW)
150
100
50
0
MS
MI
DI
B
Shoot total GSH content (nmol/g FW)
400
300
200
100
0
C
Shoot GSH:GSSG ratio
15
10
5
0
Col-0
cad2-1
pad2-1
D
Root Fe content (µg/g FW)
250
200
150
100
50
E
Root total GSH content (nmol/g FW)
F
Root GSH:GSSG ratio

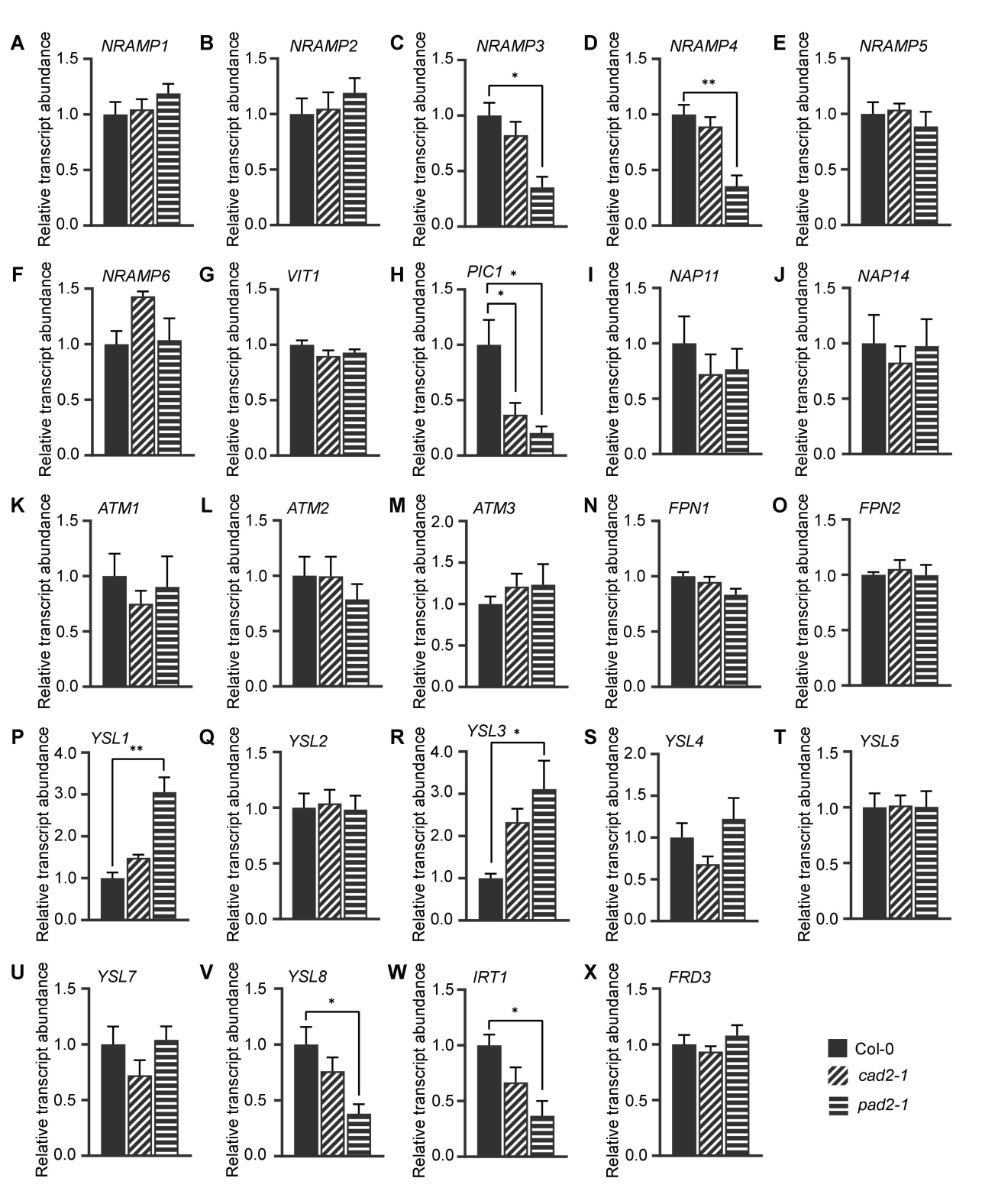
A
NRAMP1
B
NRAMP2
C
NRAMP3
D
NRAMP4
E
NRAMP5
F
NRAMP6
G
VIT1
H
PIC1
I
NAP11
J
NAP14
K
ATM1
L
ATM2
M
ATM3
N
FPN1
O
FPN2
P
YSL1
Q
YSL2
R
YSL3
S
YSL4
T
YSL5
U
YSL7
V
YSL8
W
IRT1
X
FRD3
Relative transcript abundance
Col-0
cad2-1
pad2-1

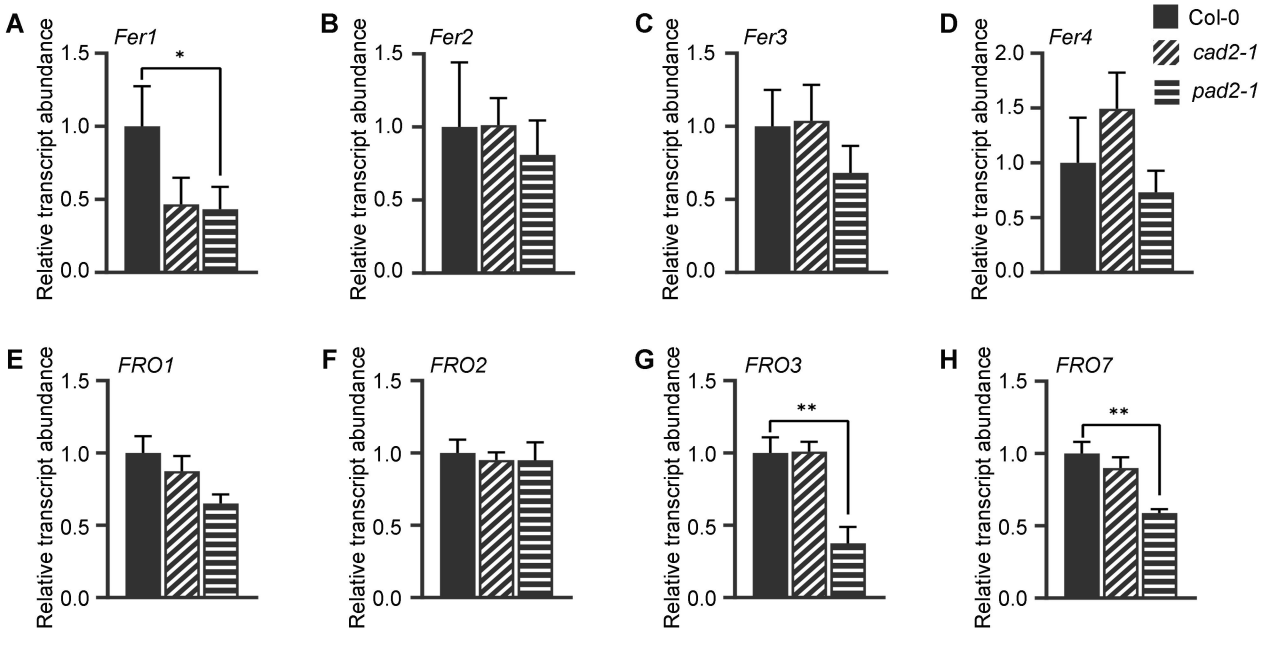
A
Fer1
Relative transcript abundance
1.5
1.0
0.5
0.0
*
B
Fer2
C
Fer3
D
Fer4
2.0
Col-0
cad2-1
pad2-1
E
FRO1
F
FRO2
G
FRO3
**
H
FRO7

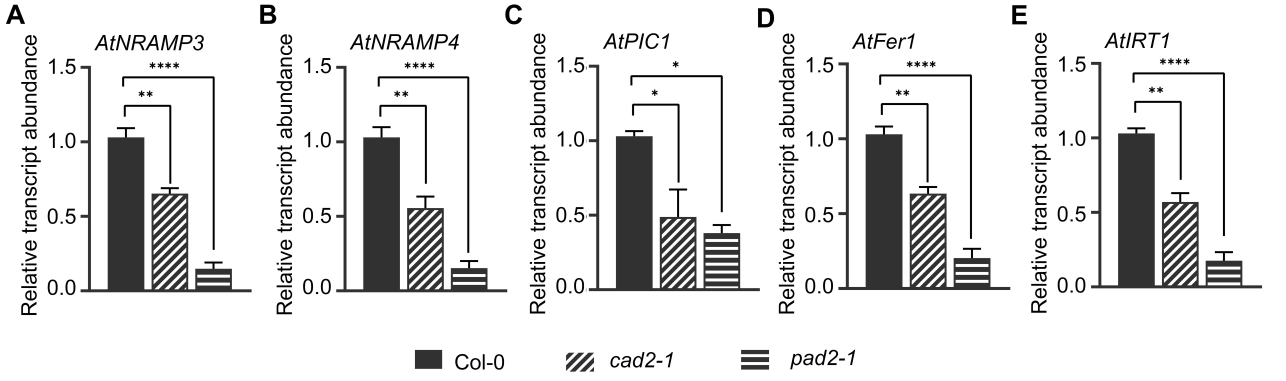
A
AtNRAMP3
B
AtNRAMP4
C
AtPIC1
D
AtFer1
E
AtIRT1
Relative transcript abundance
1.5
1.0
0.5
0.0
****
**
*
Col-0
cad2-1
pad2-1

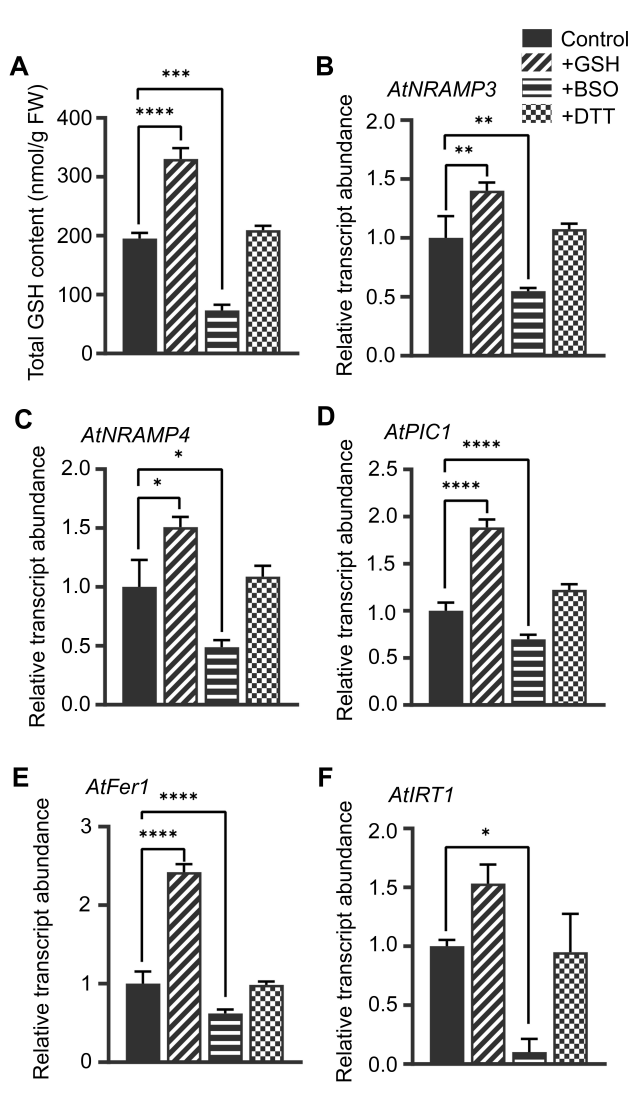
Control
+GSH
+BSO
+DTT
A
Total GSH content (nmol/g FW)
400
300
200
100
0
****
***
B
AtNRAMP3
Relative transcript abundance
2.0
1.5
1.0
0.5
0.0
**
**
C
AtNRAMP4
Relative transcript abundance
2.0
1.5
1.0
0.5
0.0
*
*
D
AtPIC1
Relative transcript abundance
2.5
2.0
1.5
1.0
0.5
0.0
****
****
E
AtFer1
Relative transcript abundance
3
2
1
0
****
****
F
AtIRT1
Relative transcript abundance
2.0
1.5
1.0
0.5
0.0
*

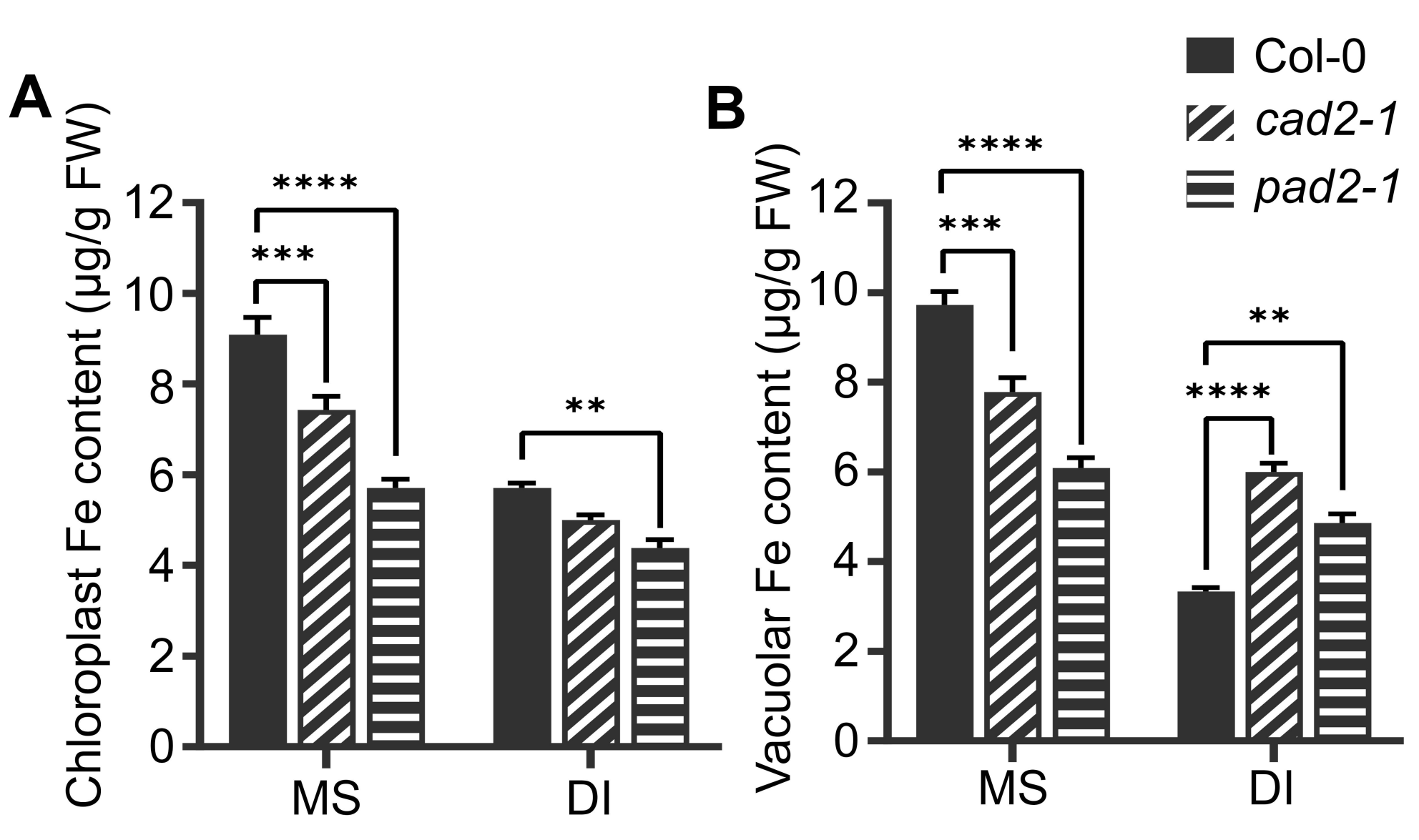
A
Chloroplast Fe content (µg/g FW)
12
10
8
6
4
2
0
****
***
**
MS
DI
B
Vacuolar Fe content (µg/g FW)
12
10
8
6
4
2
0
****
***
**
****
MS
DI
Col-0
cad2-1
pad2-1

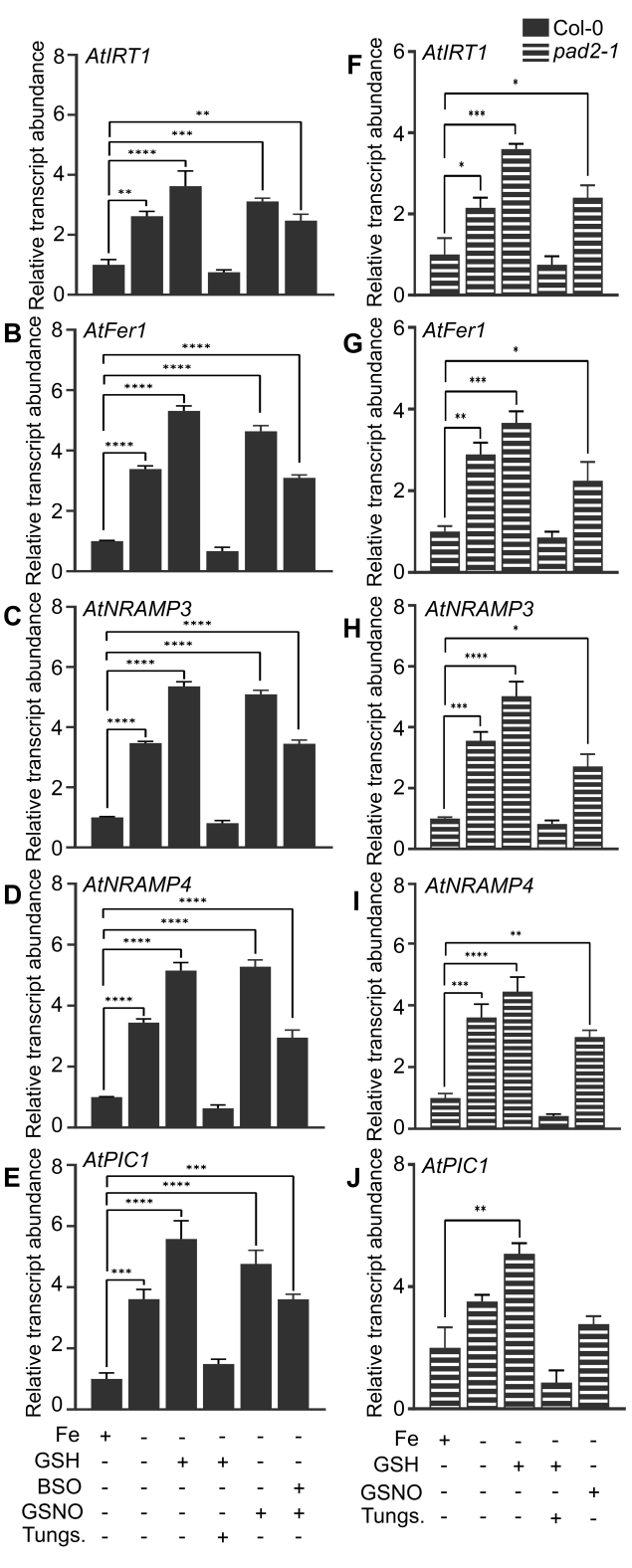
Col-0
pad2-1
A
AtIRT1
B
AtFer1
C
AtNRAMP3
D
AtNRAMP4
E
AtPIC1
F
AtIRT1
G
AtFer1
H
AtNRAMP3
I
AtNRAMP4
J
AtPIC1
Relative transcript abundance
Fe + - - - - -
GSH - - + + - -
BSO - - - - - +
GSNO - - - - + +
Tungs. - - - + - -
Fe + - - - -
GSH - - + + -
GSNO - - - - +
Tungs. - - - + -

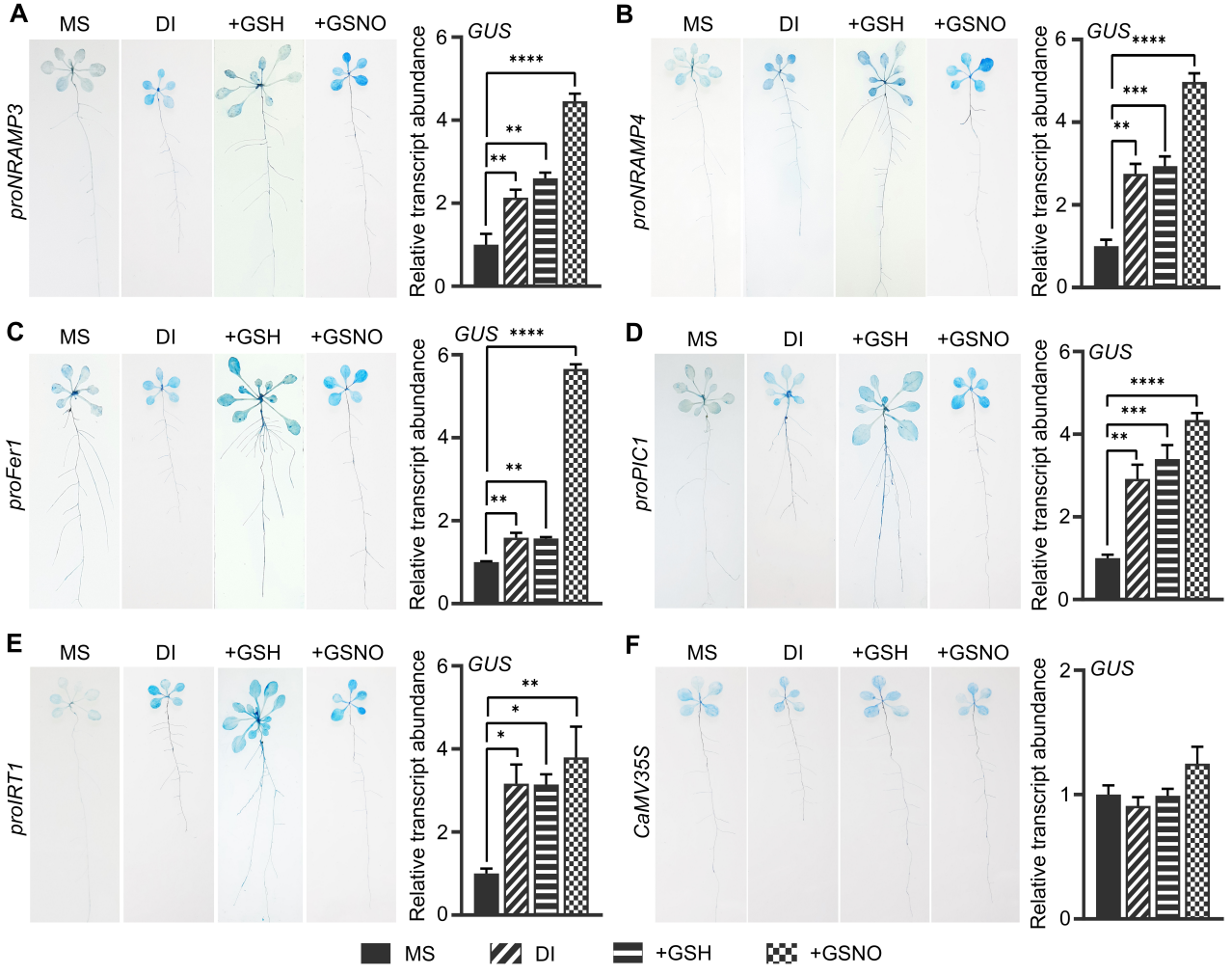
A
MS
DI
+GSH
+GSNO
proNRAMP3
GUS
Relative transcript abundance
0
2
4
6
**
**
****
B
proNRAMP4
C
proFer1
D
proPIC1
E
proIRT1
*
*
**
F
CaMV35S
MS
DI
+GSH
+GSNO

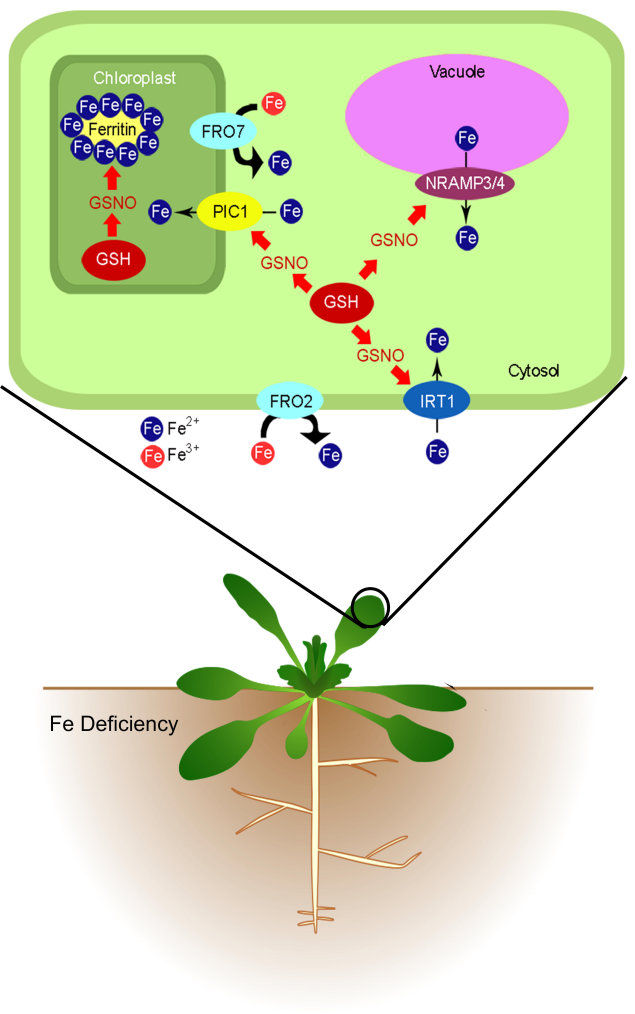
Chloroplast
Fe Fe Fe
Fe Ferritin Fe
Fe Fe Fe Fe
GSNO
GSH
Fe
FRO7
Fe
Fe
PIC1
Fe
Vacuole
Fe
NRAMP3/4
Fe
GSNO
GSNO
GSH
GSNO
Fe
IRT1
Fe
Cytosol
FRO2
Fe
Fe
Fe Fe2+
Fe Fe3+
Fe Deficiency